

In the year 1900 Max PLANCK postulated – at the beginning very reluctantly – an energy packet $W = h\nu$, today known as the “photon”. In 1905, the famous “annus mirabilis” of EINSTEIN, classical physics finally broke down: EINSTEIN explained the photoelectric effect based on PLANCK’s quantum of action h , he also formulated the theory of special relativity, declared the equivalence of mass and energy, and presented an atomistic explanation of BROWN’s motion. However, only in the middle the 1950ies – nearly 50 years later – quantum optics came to life and remains a very active field of modern research until now. The present chapter gives a first introduction into some of its basics.

Overview

After the previous extensive exploration into the wave character of light, the present chapter focuses on its particle properties and on the statistical properties of photons. In Sect. 2.1 concepts such as “quasi-monochromatic” and “partially coherent” light will be defined and exemplified by simple models for a laser and a classical light source. We shall familiarize ourselves with the fundamental experiments, beginning with the famous “Hanbury BROWN-TWISS experiment”. In Sect. 2.2 we shall try to find a pragmatic approach to the quantum mechanical description of photon states – giving an introduction for “pedestrians” so to say. Finally, we shall in Sect. 2.3 apply the new tools to the theory of absorption and emission of light – this time with explicit consideration of the quantum nature of photons. This will allow us for the first time to *derive* the basic formulas for spontaneous emission – as opposed to the previous, hand waving introduction of this inherently quantum mechanical phenomenon.

2.1 Some Basics for Quantum Optics

2.1.1 Introduction

Ground breaking work on the quantum statistics of light has been carried out in 1954 and the following years. Of fundamental importance are the experiments of R. Hanbury BROWN¹ and R.Q. TWISS (1954, 1956a, 1956b, 1958). Roy J. GLAUBER was one of the pioneers of theoretical quantum statistics (see e.g. GLAUBER 1963) and received the NOBEL prize for his work 2005 – together with John HALL and Ted HÄNSCH as already noted in the context of precision spectroscopy and frequency combs. The work of GLAUBER provides much of the essential theoretical background for the present chapter.

We start by describing a *continuous light source*, be it a laser beam whose light is not strictly monochromatic, be it a completely chaotic light source such as an incandescent bulb, our sun, or a fluorescent lamp. It has a finite bandwidth $\delta\omega_c$ around a central frequency ω_c , and is called *quasi-monochromatic*, if

$$\delta\omega_c \ll \omega_c. \quad (2.1)$$

We shall see that the concept of quasi-monochromaticity is closely related to *coherence* or *partial coherence* onto which this section will focus, and which we shall meet time and again later on. For further details we refer the interested reader to the standard work of LOUDON (2000), by which much of this chapter has been inspired, as well as to WEISSBLUTH (1989) and the more recent monograph by LAMBROPOULOS and PETROSYAN (2007) who also give many further references.

We now deal with continuous light beams which can no longer be described in a neat analytic form as wave-packets. Nevertheless, these light beams are still capable to generate typical interference structures, similar to those reported for light pulses in Sect. 1.5. The property that both have in common is quantified by the *degree of coherence*.

2.1.2 First-Order Degree of Coherence

Correlation functions have already been introduced in Sect. 1.5.2, and more details are found in Appendix G.2, Vol. 1. Now we shall use these correlation functions to characterize the *coherence properties* of electromagnetic radiation. For the field amplitude $E^+(t) = (E^-(t))^*$ as defined by (1.36) we write²

¹The experiment is usually referred to as “Hanbury BROWN-TWISS Experiment”, but one should know that “Hanbury” is a first name, and the second author’s name is “Twiss”.

²Note that this definition differs slightly from LOUDON (2000) ($\delta \rightarrow -\delta$) who uses a somewhat unconventional definition of the FOURIER transform.

$$G^{(1)}(\delta) = \langle E^-(t)E^+(t+\delta) \rangle \quad (2.2)$$

$$= \int_{-\infty}^{\infty} E^-(t)E^+(t+\delta)dt \quad \text{for a pulse, and} \quad (2.3)$$

$$= \frac{1}{T_{\text{av}}} \int_{-T_{\text{av}}/2}^{T_{\text{av}}/2} E^-(t)E^+(t+\delta)dt \quad \text{for a CW source.} \quad (2.4)$$

The mode of averaging $\langle \dots \rangle$ depends on the specific case. Note that the averaging time T_{av} for the CW case has to be sufficiently long, so that $G^{(1)}(\delta)$ does no longer change when T_{av} is extended. As just defined, the dimension of $G^{(1)}(\delta)$ depends on the case (pulse or CW). Thus it is advantageous to introduce the dimensionless *first-order degree of temporal coherence*:

$$g^{(1)}(\delta) = \frac{\langle E^-(t)E^+(t+\delta) \rangle}{\langle E^-(t)E^+(t) \rangle} = \frac{\langle E^-(t-\delta)E^+(t) \rangle}{\langle E^-(t)E^+(t) \rangle} = g^{(1)}(-\delta)^* \quad (2.5)$$

$$\text{with } 0 \leq |g^{(1)}(\delta)| \leq 1.$$

In general $g^{(1)}(\delta)$ is complex and $|g^{(1)}(\delta)|$ gives a quantitative measure of coherence. It determines how far the field $E^+(t)$ and its displaced image $E^+(t+\delta)$ may be separated in time and still have a memory of each other. If they fully overlap $g^{(1)}(0) = 1$ and the light is said to be fully coherent, if they are far apart $g^{(1)}(\infty) = 0$ the light is incoherent.

In the case of a wave-packet (1.107), with an envelope $E_0 h(t)$ according to (1.109), the degree of coherence with (2.2) becomes simply

$$g^{(1)}(\delta) = e^{i\omega_c \delta} \int_{-\infty}^{\infty} h(t)h(t+\delta)dt / \int_{-\infty}^{\infty} h^2(t)dt. \quad (2.6)$$

Note that $h(t)$ is an analytic, square integrable function, representing a pulse or a finite sequence of pulses. Using the WIENER-KHINCHIN *theorem* (I.17), Vol. 1 for the FOURIER transform of auto-correlation function of the field, we may write the intensity spectrum:

$$\tilde{I}(\omega) = \frac{\varepsilon_0 c}{4\pi} |\tilde{E}^+(\omega)|^2 = \frac{\varepsilon_0 c}{4\pi} \int_{-\infty}^{\infty} e^{-i\omega \delta} d\delta \int_{-\infty}^{\infty} E^-(t)E^+(t+\delta)dt. \quad (2.7)$$

For normalization we can use the fluence of the light source

$$F = \int_{-\infty}^{\infty} I(t)dt = \frac{\varepsilon_0 c}{2} \int_{-\infty}^{\infty} E^-(t)E^+(t)dt = I_0 \int_{-\infty}^{\infty} h^2(t)dt, \quad (2.8)$$

with $I_0 = \varepsilon_0 c E_0^2/2$. Inserting this into (2.7) and applying the definition (2.5) of $g^{(1)}(\delta)$ we obtain

$$\tilde{I}(\omega) = \frac{F}{2\pi} \int_{-\infty}^{\infty} g^{(1)}(\delta) e^{-i\omega \delta} d\delta. \quad (2.9)$$

Thus, the *intensity spectrum* is given by the inverse FOURIER transform of the *first-order degree of temporal coherence* of a light source.

It is also useful to recall the units $[\tilde{I}(\omega)] = \text{J s m}^{-2}$, while $\int_{-\infty}^{\infty} \tilde{I}(\omega) d\omega = F$ (which is easily verified from Eq. (2.9)) has indeed the unit $[F] = \text{J m}^{-2}$.

Specifically for a Gaussian pulse with the field amplitude (1.110), one finds from the convolution (2.6)

$$g^{(1)}(\delta) = e^{i\omega_c \delta} e^{-\frac{1}{2}(\frac{\delta}{\tau_G})^2}. \quad (2.10)$$

With this and (2.9) the intensity spectrum of a Gaussian pulse follows (see also Appendix I.4.1 in Vol. 1):

$$\tilde{I}(\omega) = \frac{F}{\omega_G \sqrt{\pi}} \exp\left[-\left(\frac{\omega - \omega_c}{\omega_G}\right)^2\right] = \frac{I_0}{\omega_G^2} \exp\left[-\left(\frac{\omega - \omega_c}{\omega_G}\right)^2\right] \quad (2.11)$$

$$\text{with } F = \sqrt{\pi/2} I_0 \tau_G, \text{ and } \omega_G = \sqrt{2}/\tau_G.$$

In contrast, for CW light the evaluation may not be that trivial, since any realistic model will have to describe a stationary light source as a random ensemble of wave-packets. It turns out to be more convenient to average in frequency space. To this end, we adapt the spectral intensity distribution (2.7) appropriately, and replace the integrals (2.3) by averages (2.4):

$$\begin{aligned} \check{I}(\omega) &= \frac{\varepsilon_0 c}{4\pi} \int_{-\infty}^{\infty} e^{-i\omega \delta} d\delta \left\{ \frac{1}{T_{\text{av}}} \int_{-T_{\text{av}}/2}^{-T_{\text{av}}/2} E^-(t) E^+(t + \delta) dt \right\} \\ &= \frac{I}{2\pi} \int_{-\infty}^{\infty} g^{(1)}(\delta) e^{-i\omega \delta} d\delta \end{aligned} \quad (2.12)$$

$$\text{with } I = \frac{\varepsilon_0 c}{2} \langle E^-(t) E^+(t) \rangle = \frac{1}{T_{\text{av}}} \int_{-T_{\text{av}}/2}^{T_{\text{av}}/2} I(t) dt. \quad (2.13)$$

We have used here the symbol $\check{I}(\omega)$ (unit $[\check{I}(\omega)] = \text{W s m}^{-2}$) for the intensity spectrum of the CW light, in order to indicate its different definition. From this follows $\int_{-\infty}^{\infty} \check{I}(\omega) d\omega = I$, which is now the *average intensity of the stationary source*, measured in units $[I] = \text{W m}^{-2}$ (rather than the fluence as in the case of a pulse).

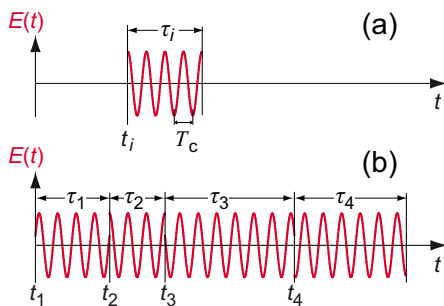
We finally invert (2.9) and (2.12) and find the useful relations by which the *first-order degree of coherence* can be derived in both cases (properly normalized) as inverse FOURIER transform of the spectrum. For pulsed and CW sources we obtain

$$g^{(1)}(\delta) = \frac{1}{F} \int_{-\infty}^{\infty} \tilde{I}(\omega) e^{i\omega \delta} d\omega \quad \text{and} \quad (2.14)$$

$$= \frac{1}{I} \int_{-\infty}^{\infty} \check{I}(\omega) e^{i\omega \delta} d\omega, \quad \text{respectively.} \quad (2.15)$$

The next two subsections are devoted to quasi-monochromatic light beams, with their degree of coherence $g^{(1)}(\delta)$ and their interference properties.

Fig. 2.1 (a) Illustration of the wave-packet described by (2.16), (b) schematic representation of the model for a stationary, quasi-monochromatic laser composed of such wave-packets (for visual clarity we have drawn T_c much too large; in reality, of course, we have $T_c \ll \tau_i$)



2.1.3 Quasi-Monochromatic Light

We recall that the laser pulses which we have discussed in the previous chapter have been introduced in Sect. 1.4.1 as *coherent superposition of plane waves* from a limited frequency range of a FWHM $\Delta\omega_{1/2}$. Such a light pulse has a finite duration $\tau \propto 1/\Delta\omega_{1/2}$. Alternatively we have described in Sect. 1.4.3 periodic pulse trains as a FOURIER series. Obviously, neither of these two descriptions can lead to a realistic model of a quasi-monochromatic and continuous laser beam, since such a CW laser radiates effectively from $t = -\infty$ to $t = +\infty$ without obvious intermission (at least for a couple of hours or days). With some effort and good electronics the frequency may be stabilized for a long time to a few Hz. Still it cannot be modelled by a plane (or Gaussian) continuous wave – nor by any kind of a wave-packet.

Such a CW light beam has to be modelled with “*stationary and ergodic statistical properties, so that ensemble averages over the probability distribution are equivalent to long-time averages over the beams in a single experiment*” (LOUDON 2000). Let us imagine – as a simple model³ – a laser beam to be composed of a large number of rectangular wave trains (see Appendix I.4.3 in Vol. 1) of constant amplitude but different, finite durations. One such wave-packet is illustrated in Fig. 2.1(a) as a function of time at a fixed position in space (without loss of generality we choose again $\mathbf{r} = 0 \Rightarrow k\mathbf{z} = 0$). Thus, in our standard notation (1.36) we have

$$E_i^+(t) = \begin{cases} E_0 e^{i(\omega_c t - \omega_c t_i - \phi_i)} & \text{for } t_i < t < t_i + \tau_i, \\ 0 & \text{else,} \end{cases} \quad (2.16)$$

and the intensity is as usual $I_0 = \varepsilon_0 c E_0^2 / 2$ in the wave-packet and zero outside. The pulse begins at $t = t_i$, it has a duration τ_i and its relative phase ϕ_i is statistically distributed. To make things not too complicated we assume, however, that the period $T_c = 2\pi/\omega_c$ (or its wavelength λ_c) is constant. Such a wave-packet may typically contain 10^8 to 10^{11} periods. The spectral intensity distribution of this pulse is given

³Similarly one has to treat any *chaotic light*, with large phase and intensity fluctuations, as e.g. emitted from a collision or DOPPLER broadened gas discharge, an incandescent bulb or an ensemble of excited atoms – even if the spectrum may be different, the bandwidth larger and the coherence time to be introduced here correspondingly shorter.

by (I.53), Vol. 1:

$$\tilde{I}_i(\omega) = \frac{I_0 \tau_i^2}{2\pi} \operatorname{sinc}^2 \left[\frac{\tau_i (\omega - \omega_c)}{2} \right] \quad \text{with } \operatorname{sinc} x = \frac{\sin x}{x}. \quad (2.17)$$

A real quasi-monochromatic light beam, which extends over large times and distances, can now be modelled by many such pulse trains as indicated in Fig. 2.1(b). They may, of course, also overlap each other. The frequency bandwidth in a **CW** laser is usually determined by mechanical and thermal instabilities of the experimental setup, such as vibrations of the mirrors, collision processes in the amplifier medium, dust particles accidentally passing the laser beam etc. These processes occur completely statistically, let us assume with a constant average rate $1/\tau_c$. We further assume that such events after the times $\tau_1, \tau_2, \dots, \tau_i$ just change the phase $\phi_1, \phi_2, \dots, \phi_i$. The amplitude is kept constant. The probability that such a wave-packet has a duration between τ_i and $\tau_i + d\tau_i$, is described by an *exponential distribution* as outlined in our elementary introduction to statistics, Sect. 1.3.1 in Vol. 1:

$$w(\tau_i) d\tau_i = \frac{1}{\tau_c} e^{-\tau_i/\tau_c} d\tau_i. \quad (2.18)$$

The average time between the phase changes is τ_c . We call it *coherence time*. The corresponding length of the wave-packet sketched in Fig. 2.1(b) is the so called *coherence length*

$$\ell_c = \tau_c c. \quad (2.19)$$

The whole light beam is described by this *statistical distribution of individual wave-packets*. Each of them is characterized by a spectral distribution according to (2.17) and an arbitrary statistical phase ϕ_i . We emphasize again, that this continuous light beam cannot be described by any kind of coherent, linear superposition of waves. Its overall spectral distribution is found as the statistical average of the individual spectral distributions for all possible durations τ_i of the wave-packets and re-normalization according to (I.32), Vol. 1. With (2.17) and (2.18) the integration can be carried out in closed form:

$$\begin{aligned} \check{I}(\omega) &= \langle \tilde{I}_i(\omega) \rangle = \frac{I_0}{2\pi \tau_c} \int_0^\infty w(\tau_i) \tau_i^2 \operatorname{sinc}^2 \left[\frac{\tau_i (\omega - \omega_c)}{2} \right] d\tau_i \\ &= \frac{\tau_c}{\pi} \frac{I}{1 + (\omega - \omega_c)^2 (\tau_c)^2} = \frac{I}{2\pi} \frac{\Delta\omega_{1/2}}{(\omega - \omega_c)^2 + (\Delta\omega_{1/2}/2)^2}, \end{aligned} \quad (2.20)$$

with a **FWHM** $\Delta\omega_{1/2} = 2/\tau_c = 2c/\ell_c$.

Thus, one finds a **LORENTZ profile**. It is normalized here so that the integration over all frequencies gives the local average intensity $I = I_0 = \varepsilon_0 c E_0^2/2$ of the laser beam (assumed to be independent of time). The profile is characterized by the coherence time τ_c . The maximum of the spectral intensity distribution (intensity per angular

Table 2.1 Coherence time τ_c and first-order degree of coherence $g^{(1)}(\delta)$ for different spectral distributions with **FWHM** $\Delta\omega_{1/2}$

	Spectrum	$\Delta\omega_{1/2}$	$g^{(1)}(\delta) \times e^{-i\omega_c\delta}$	$g^{(1)}(\tau_c)$
Lorentzian ^a	$[\tau_c^2(\omega - \omega_c)^2 + 1]^{-1}$	$2/\tau_c$	$\exp[- \delta /\tau_c]$	$1/e$
Gaussian ^b	$\exp[-\tau_c^2(\omega - \omega_c)^2]$	$2\sqrt{\ln 2}/\tau_c$	$\exp[-(\delta/\tau_c)^2]$	$1/e$
Rectangle	1 for $-\frac{\pi}{\tau_c} \leq \omega - \omega_c \leq \frac{\pi}{\tau_c}$	$2\pi/\tau_c$	$\text{sinc}(\pi\delta/\tau_c)$	0

^aNote that this definition for the LORENTZ profile differs slightly from (5.8), Vol. 1, used there for spontaneous emission with a **FWHM** of $\Delta\omega_{1/2} = 1/\tau_{\text{nat}}$

^bCoherence time and the usual Gaussian time are related by $\tau_c = \sqrt{2}\tau_G$

frequency) at $\omega = \omega_c$ is

$$\check{I}(\omega_c) = \frac{2I}{\pi \Delta\omega_{1/2}}. \quad (2.21)$$

For the *first-order degree of temporal coherence* (2.5) one obtains

$$g^{(1)}(\delta) = e^{i\omega_c\delta} e^{-|\delta|/\tau_c} \quad (2.22)$$

for the LORENTZ profile (2.20), as can easily be verified with (2.12).

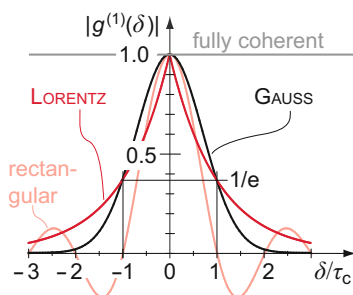
By way of example, a continuous dye laser (often used in spectroscopy) may provide an intensity $I \simeq 1 \text{ W cm}^{-2}$ with a typical bandwidth of $\Delta\nu_{1/2} \simeq 1 \text{ MHz}$. Coherence time and coherence length are then $\tau_c \simeq 320 \text{ ns}$ and $\ell_c \simeq 100 \text{ m}$, respectively. The peak spectral intensity is $\check{I}(\omega_c) \simeq 5 \times 10^{-8} \text{ W cm}^{-2} \text{ s}$. We may compare this to the spectral intensity of the sun at 555 nm which according to (1.85), Vol. 1 is $\check{I}(\omega_c) \simeq 3.5 \times 10^{-12} \text{ W s cm}^{-2}$ (at the surface of the sun!).

The above description of a quasi-monochromatic light beam is just one possible model. In principle, one has to start from a detailed analysis of a given experimental situation. A variety of wave-packets differing from those shown in Fig. 2.1 are conceivable. In any case, $g^{(1)}(\delta)$ and the spectral distribution $\check{I}(\omega)$ are related by (2.12)–(2.15). If e.g., the radiation source is mainly DOPPLER broadened, it will be characterized by a distribution of frequencies corresponding to a *Gaussian* with statistically distributed phases. The corresponding degree of coherence will be the same as that derived for the Gaussian *pulse* (2.10) and the coherence time is then $\tau_c = \sqrt{2}\tau_G$.

The definition of a coherence time τ_c (or the coherence length $\ell_c = c\tau_c$) must, inevitably, be somewhat arbitrary. We shall use the time for which $g^{(1)}(\tau_c) = 1/e$, unless it passes through $g^{(1)}(\tau_c) = 0$ at a finite delay time, in which case that time is taken.

In Table 2.1 we summarize the spectra and first-order coherence properties for three important cases of quasi-monochromatic light. Their first-order degree of coherence is plotted in Fig. 2.2 as a function of delay time δ . They are compared with strictly monochromatic light ($\check{I}(\omega) \propto \delta(\omega - \omega_c)$) which – in contrast to the three statistical light sources – shows no fluctuations at all, i.e. $|g^{(1)}(\delta)| \equiv 1$ holds independent of δ .

Fig. 2.2 Magnitude of the first-order degree of coherence, $|g^{(1)}(\delta)|$, for chaotic light with a coherence time τ_c . Compared are light sources with Gaussian, Lorentzian and rectangular spectral profiles; they are confronted with a fully coherent wave (infinite coherence time) $|g^{(1)}(\delta)| = 1$



2.1.4 Temporal or Longitudinal Coherence

To develop the concept of coherence further, we return to interference experiments as discussed in Sect. 1.5.3 and apply the just defined first-order degree of coherence. This will also be a useful preparation for later discussions of polarization and state distribution in atoms (Chap. 9).

Let us take a closer look on first-order coherence observed e.g. in YOUNG's double slit experiment, or in a MICHELSON interferometer. Here, as a first step, we idealize the light beam and assume it to be parallel (e.g. originating from a point like source). In Fig. 2.3 the key elements of such an experiment are illustrated very schematically. The electric field $\mathbf{E}(\mathbf{r}, t)$ is split into two parts, $\mathbf{E}(\mathbf{r}_1, t)$ and $\mathbf{E}(\mathbf{r}_2, t)$, i.e. by a double slit in the diffraction experiment, or with the help of a beam splitter in the interferometer experiment. Both rays A and B propagate along different optical pathways s_1 and s_2 , respectively – be it due to diffraction, changes of the index of refraction or just due different distances. This leads to a time delay δ between the two partial beams. Finally, both parts are superposed and interfere – effectively at different individual times, t_1 and t_2 . Using the terminology (1.36), we write

$$\mathbf{E}^+(\mathbf{r}, t) = [a_1 \mathbf{E}^+(\mathbf{r}_1, t_1) + a_2 \mathbf{E}^+(\mathbf{r}_2, t_2)].$$

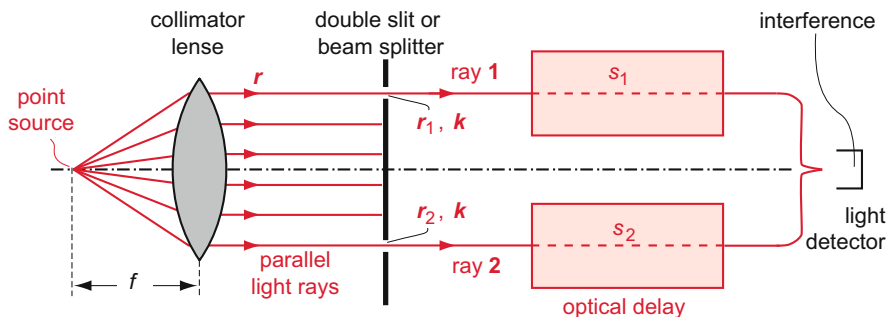


Fig. 2.3 Very schematic layout of an interference experiment with two parallel light rays originating from a point like light source; the brace on the right just indicates that the two rays are made to interfere – it does not sketch a light path

The prefactors a_1 and a_2 account for the fact the ray A and B are only a fraction of the beam and may even be further reduced before reaching the detector. If only ray A or only ray B were present, the signals would be

$$\begin{aligned} I_1 &= \frac{\varepsilon_0 c}{2} a_1^2 |E^+(\mathbf{r}_1, t_1)|^2 = a_1^2 I \quad \text{or} \\ I_2 &= \frac{\varepsilon_0 c}{2} a_2^2 |E^+(\mathbf{r}_2, t_2)|^2 = a_2^2 I, \quad \text{respectively,} \end{aligned} \quad (2.23)$$

with I being the averaged total intensity of the original beam. For a first-order process ($\mathcal{N} = 1$) we write the averaged time dependent intensity (1.134) at the detector as

$$I(\mathbf{r}, t) = \frac{\varepsilon_0 c}{2} E^-(\mathbf{r}, t) E^+(\mathbf{r}, t) = I_1 + I_2 + I_{12}. \quad (2.24)$$

The interference term in which we are mostly interested, is given by

$$\begin{aligned} I_{12} &= C^2 [E^-(\mathbf{r}_1, t_1) E^+(\mathbf{r}_2, t_2) + E^+(\mathbf{r}_1, t_1) E^-(\mathbf{r}_2, t_2)] \\ &= 2C^2 \operatorname{Re}[E^-(\mathbf{r}_1, t_1) E^+(\mathbf{r}_2, t_2)] \quad \text{with } C^2 = \frac{\varepsilon_0 c}{2} a_1 a_2, \\ t_1 &= t - \frac{s_1}{c}, \quad t_2 = t - \frac{s_2}{c} = t_1 + \delta, \quad \text{and } \delta = \frac{s_1 - s_2}{c}. \end{aligned} \quad (2.25)$$

The expected pattern is a function of the relative phase $\omega\delta$ between rays A and B. Since partially coherent light with a coherence time τ_c has a bandwidth $\Delta\omega \simeq 1/\tau_c$ of different frequencies, one expects the interference structure to smear out when $\Delta\omega\delta \geq \pi$, i.e. if $\delta \geq \pi\tau_c$. The detector usually integrates over times $\gg \tau_c$.

For a quantitative evaluation we have to keep in mind, that in any model of quasi-monochromatic light the electric field will be described as a statistical ensemble of many individual wave-packets $E_i^+(\mathbf{r}, t)$, e.g. as described by (2.16). Thus, we have to average the interference term in (2.24) temporally – or to find the ensemble average. It turns out that this is done most conveniently in frequency space: we rewrite the interference term (2.25) by using the (inverse) FOURIER transform (1.106), with $\tilde{E}^+(\mathbf{k})$ being independent of the direction of \mathbf{k} (parallel light with $k = \omega/c$):

$$I_{12} = 2 \left(\frac{C}{2\pi} \right)^2 \left\langle \int d\omega \int d\omega' (\tilde{E}_i^+(\omega))^* e^{i(\mathbf{k} \cdot \mathbf{r}_1 - \omega t_1)} \tilde{E}_j^+(\omega') e^{-i(\mathbf{k}' \cdot \mathbf{r}_2 - \omega' t_2)} \right\rangle. \quad (2.26)$$

Obviously, only $\tilde{E}_i^-(\omega) \tilde{E}_j^+(\omega')$ is affected by the statistical averaging over wave-packets. We also observe that each of the wave-packets i and j carries its own statistical phase ϕ_i or ϕ_j , respectively – as exemplified by (I.51), Vol. 1. Thus, these complex quantities are distributed at random on a circle in the complex plane – and hence they average out over the whole ensemble. Only those terms which are caused by the same wave-packet $i = j$ contribute to (2.26). Somewhat laxly one says:

Each photon interferes only with itself.

We also note that $\tilde{E}_i^-(\omega)E_i^+(\omega')$ according to (I.51), Vol. 1 contains the function $\exp[i(\omega - \omega')t_i]$. Averaging over the statistically distributed starting times t_i (i.e. integrating over all times t_i) lets all terms with $\omega' \neq \omega$ disappear. Thus

$$\langle (\tilde{E}_i^+(\omega))^* \tilde{E}_j^+(\omega') \rangle = 2\pi \delta_{ij} \delta(\omega - \omega') \langle |\tilde{E}_i^+(\omega)|^2 \rangle. \quad (2.27)$$

In summary, the ensemble average of the interference term (2.26) is simply

$$\begin{aligned} I_{12} &= 2 \frac{C^2}{2\pi} \operatorname{Re} \int d\omega e^{i\mathbf{k} \cdot (\mathbf{r}_1 - \mathbf{r}_2)} e^{i\omega(t_2 - t_1)} \langle |\tilde{E}_i^+(\omega)|^2 \rangle \\ &= 2a_1 a_2 \operatorname{Re} \int d\omega e^{i\mathbf{k} \cdot (\mathbf{r}_1 - \mathbf{r}_2)} e^{i\omega(t_2 - t_1)} \langle \tilde{I}_i(\omega) \rangle, \end{aligned} \quad (2.28)$$

where we have used (I.32), Vol. 1. With $\mathbf{k} \perp (\mathbf{r}_1 - \mathbf{r}_2)$ in our model geometry Fig. 2.3, and with the time delay $t_2 - t_1 = \delta$ we obtain the sought-after interference term as:

$$\begin{aligned} I_{12} &= 2C^2 \operatorname{Re} \langle E^-(\mathbf{r}_1, t_1) E^+(\mathbf{r}_2, t_2) \rangle \\ &= 2a_1 a_2 \operatorname{Re} \int e^{i\omega\delta} \check{I}(\omega) d\omega = 2\sqrt{I_1 I_2} \operatorname{Re}[g^{(1)}(\delta)]. \end{aligned} \quad (2.29)$$

$\check{I}(\omega) = \langle \tilde{I}_i(\omega) \rangle$ is the ensemble averaged intensity spectrum. In the last step, using (2.15), we have identified the resulting integral as the *first-order degree of (longitudinal) coherence* and use the abbreviations (2.23).

For quasi-monochromatic light with a carrier frequency ω_c the first-order degree of coherence always assumes the form $\pm |g^{(1)}(\delta)| \exp(i\omega_c \delta)$ (see the examples given in Table 2.1). Thus, inserting (2.29) into (2.24) we obtain the interference signal (first-order) as a function of the delay time δ :

$$I(\delta) = I_1 + I_2 \pm 2\sqrt{I_1 I_2} |g^{(1)}(\delta)| \cos \omega_c \delta. \quad (2.30)$$

We emphasize that the above derivation is characteristic for any kind of quasi-monochromatic light composed of an ensemble of wave-packets with statistically distributed phases. The $|g^{(1)}(\delta)|$ is the *quantitative measure for temporal coherence* we have been looking for. One calls this property *temporal coherence* or *longitudinal coherence*, since coherence time and coherence length are directly related by $\ell_c = c\tau_c$: ℓ_c gives the distance by which a wave-packet may be displaced from its image so that the degree of coherence decreases to $1/e$.

Some Examples In practice, interference fringes often show less contrast than expected from (2.30) where $\operatorname{Re}[g^{(1)}(0)] = 1$. Instrumental imperfections or spatial incoherences can be responsible, as we shall discuss Sect. 2.1.7. To quantify this reduction of contrast one introduces a parameter

$$\text{visibility}, \quad V = \frac{I_{\max} - I_{\min}}{I_{\max} + I_{\min}}, \quad (2.31)$$

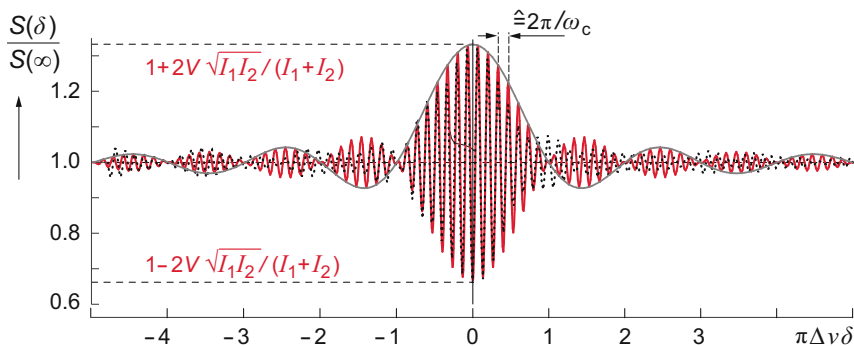


Fig. 2.4 Interference pattern for two rays with a rectangular spectrum according to (2.32). The dotted line represents suitably processed experimental data, measured at the CHARA high resolution stellar interferometer array, extracted from TEN BRUMMELAAR et al. (2005). The full black line is proportional to $\text{sinc}(\pi \Delta \nu \delta)$

by which the interference term in (2.30) has to be multiplied. Visibility can be measured by registering $I(\delta)$ in a delay scan. It may contain valuable information about the light source as we shall discuss in Sects. 2.1.7–2.1.8. In the following we assume for an ideal interferometric measurement $I_1 = I_2$ and normalize the signal to the uncorrelated limit $I(\infty)$. Finally, the expressions given in Table 2.1 have to be inserted.

First we consider a rather broad band **CW light source** which is passed through a narrow-band spectral filter, as done e.g. in stellar interferometry. If the filter has a rectangular profile with a bandwidth $\Delta\omega$ as described in Appendix I.4.4, Vol. 1, we obtain from (2.14) and (I.56), Vol. 1 $\text{Re}[g^{(1)}(\delta)] = \text{sinc}(\Delta\omega\delta/2) \cos \omega_c\delta$. The normalized interference signal is thus

$$\frac{I(\delta)}{I(\infty)} = 1 + 2V \text{sinc}(\Delta\omega\delta/2) \cos \omega_c\delta. \quad (2.32)$$

Figure 2.4 shows such an interference pattern. For reference we note that the fringes vanishes for the first time at $\Delta\omega\delta/2 = \pi \Delta\nu\delta$, with $\Delta\nu$ given in frequency units. The fringes are caused by the $\cos \omega_c\delta$ term in (2.32) and depend on the phase difference $\omega_c\delta = k(s_1 - s_2)$ between rays 1 and 2. The contrast clearly changes with delay time and is given by $V \times |g^{(1)}(\delta)|$. It has its maximum for $\delta = 0$ where $|g^{(1)}(\delta)| = 1$, while it disappears for long delay times. To compare the above theoretical derivation with some real experiment, we show in Fig. 2.4 a “fringe scan” extracted from one of the first publications of the CHARA optical/infrared interferometric array located on Mount Wilson, CA (TEN BRUMMELAAR et al. 2005). The spectra were taken in the K band at $2.133\mu\text{m}$ with one of their 15 very long baseline interferometers. The agreement with (2.32) is impressive, albeit – as expected with such simple modelling – not perfect. We shall come back to these experiments in Sect. 2.1.8.

For the *quasi-monochromatic light model* introduced in the previous subsection, the spectrum $\tilde{I}(\omega)$ is a LORENTZ distribution (2.20). Its first-order degree of coher-

ence $g^{(1)}(\delta)$ is given by (2.22). Thus, the interference pattern (2.30) becomes

$$\frac{I(\delta)}{I(\infty)} = 1 + 2V e^{-|\delta|/\tau_c} \cos \omega_c \delta. \quad (2.33)$$

We recall: the coherence time τ_c corresponds here to the average duration of the wave-packets which define the temporal properties of the quasi-monochromatic light.

If the light originates from a DOPPLER broadened (*Gaussian*) source, with (2.10) the interference pattern (2.30) becomes

$$\frac{I(\delta)}{I(\infty)} = 1 + 2V e^{-\frac{1}{2}(\frac{\delta}{\tau_G})^2} \cos \omega_c \delta. \quad (2.34)$$

2.1.5 Higher-Order Degree of Coherence

To extend the concept “degree of coherence” introduced in Sect. 2.1.2 one defines a general *degree of coherence of \mathcal{N} th order* as

$$g^{(\mathcal{N})}(\mathbf{r}_1, t_1, \dots, \mathbf{r}_{\mathcal{N}}, t_{\mathcal{N}}, \dots, \mathbf{r}_{2\mathcal{N}}, t_{2\mathcal{N}}) \quad (2.35)$$

$$= \frac{\langle E^-(\mathbf{r}_1, t_1) \dots E^-(\mathbf{r}_{\mathcal{N}}, t_{\mathcal{N}}) E^+(\mathbf{r}_{\mathcal{N}+1}, t_{\mathcal{N}+1}) \dots E^+(\mathbf{r}_{2\mathcal{N}}, t_{2\mathcal{N}}) \rangle}{[\langle |E^+(\mathbf{r}_1, t_1)|^2 \rangle \dots \langle |E^+(\mathbf{r}_{\mathcal{N}}, t_{\mathcal{N}})|^2 \rangle \dots \langle |E^+(\mathbf{r}_{2\mathcal{N}}, t_{2\mathcal{N}})|^2 \rangle]^{-1/2}},$$

with $|E^+(\mathbf{r}_{\mathcal{N}}, t_{\mathcal{N}})|^2 \equiv E^-(\mathbf{r}_{\mathcal{N}}, t_{\mathcal{N}}) E^+(\mathbf{r}_{\mathcal{N}}, t_{\mathcal{N}}) \propto I(\mathbf{r}_{\mathcal{N}}, t_{\mathcal{N}})$.

For details the interested reader is referred to the specialized literature (see e.g. LOUDON 2000; GLAUBER 2006). In the following we refer again to the dependence on time t only – which may be replaced by $t - \mathbf{r}\mathbf{k}/\omega$ if the \mathbf{r} is explicitly needed – and discuss some basic aspects of the particularly important *second-order degree of temporal coherence*

$$g^{(2)}(\delta) = \frac{\langle I(t)I(t+\delta) \rangle}{\langle I(t) \rangle^2} = \frac{\langle E^-(t)E^-(t+\delta)E^+(t)E^+(t+\delta) \rangle}{\langle E^-(t)E^+(t) \rangle^2}, \quad (2.36)$$

where the brackets $\langle \dots \rangle$ again imply the same kind of averaging as in (2.2)–(2.4). The symmetry relation is now somewhat simpler than (2.5):

$$g^{(2)}(\delta) = g^{(2)}(-\delta). \quad (2.37)$$

However, while for the first-order degree of coherence the limits $0 \leq g^{(1)}(\delta) \leq 1$ hold, no general upper limit exists for $g^{(2)}(\delta)$. Still, one may show that

$$0 \leq g^{(2)}(\delta) \quad \text{and} \quad \text{for } \delta = 0: \quad 1 \leq g^{(2)}(0) \leq \infty.$$

The latter follows from the CAUCHY-SCHWARZ inequality,⁴ which leads to $I^2 = \langle I(t) \rangle^2 \leq \langle I(t)^2 \rangle$.

Physically $g^{(2)}(\delta)$ represents the correlation function of the light intensity, i.e. it answers the question whether fluctuation in the light intensity is completely random or whether there is some kind of memory effect. In a quantum picture the photon flux, $I(t)/\hbar\omega \propto w(t)$ is proportional to probability for a photon to arrive (at time t) per unit of time, and $g^{(2)}(\delta)$ gives the probability $w(t)w(t+\delta)$ for two photons to arrive with a specific time delay: do the photons arrive completely at random or perhaps with an enhanced probability to come in pairs? At first thought this appears a strange question. Why should it be more probable to find two photons at once than at random – if the light is otherwise completely chaotic?

We cannot go into details of the statistics of chaotic light sources, but let us glance over the key arguments. We recall the model of a chaotic light source presented in Sect. 2.1.3 and assume the light to originate from many atoms. They all contribute with their individual electric field $E_j^+(t)$, each characterized by its own statistical phase. The overall field is thus given by

$$E^+(t) = \sum_i E_i^+(t).$$

Using this expression one derives the second-order correlation function (i.e. the nominator in Eq. (2.36))

$$G^{(2)}(\delta) = \langle I(t)I(t+\delta) \rangle = \langle E^-(t)E^-(t+\delta)E^+(t)E^+(t+\delta) \rangle. \quad (2.38)$$

Since uncompensated phases cancel out statistically in the averaging process, again only those terms are kept, where the field from each atom is multiplied by its own conjugate complex (at time t or $t+\delta$). However, since now the products of *four amplitudes* are involved, and a large number of atoms participates, the remaining, dominant terms are those which *arise from two pairs* of atoms $i \neq j$:

$$\langle E_i^-(t)E_i^+(t)E_j^-(t+\delta)E_j^+(t+\delta) \rangle = \langle I_i(t) \rangle \langle I_j(t+\delta) \rangle \quad \text{and} \quad (2.39)$$

$$\langle E_i^-(t)E_i^+(t+\delta)E_j^-(t)E_j^+(t) \rangle = \langle E_i^-(t)E_i^+(t+\delta) \rangle \langle E_j^-(t)E_j^+(t) \rangle. \quad (2.40)$$

As the average intensity \bar{I} in a stationary source is independent of time, the first line is simply $= \bar{I}^2$. In the second line we recognize the first-order correlation function (2.5) and its complex conjugate. Thus, in its normalized form (2.36) becomes

$$g^{(2)}(\delta) = 1 + |g^{(1)}(\delta)|^2. \quad (2.41)$$

⁴The CAUCHY-SCHWARZ inequality may be written in an easy to comprehend relation between \mathcal{N} dimensional vectors: $|\mathbf{a} \cdot \mathbf{b}|^2 \leq |\mathbf{a}|^2 \cdot |\mathbf{b}|^2$. If one chooses the intensities $I(t_j)$ as components of a vector \mathbf{a} and 1 as components of \mathbf{b} , the latter relation follows immediately.

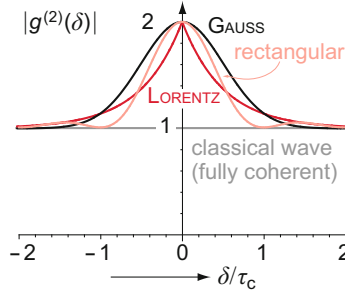


Fig. 2.5 Second order degree of temporal for chaotic light. Compared are light sources with a spectral distribution of LORENTZ, GAUSS and rectangular type. All are assumed to have equal coherence time τ_c , i.e. the delay time δ is given in units of the coherence time. They are contrasted with a classical source of radiation such as a **CW** laser of very large coherence length or an **RF** generator

Specifically, for light with a Lorentzian or Gaussian type of spectrum the second-order degree of temporal coherence (2.36) becomes

$$g^{(2)}(\delta) = 1 + \exp(-2|\delta|/\tau_c), \quad \text{and} \quad (2.42)$$

$$g^{(2)}(\delta) = 1 + \exp(-2\delta^2/\tau_c^2) = 1 + \exp(-\delta^2/\tau_G^2), \quad \text{respectively.} \quad (2.43)$$

These functions are illustrated schematically in Fig. 2.5. We recall that the correlation times τ_c are related to the respective spectral distributions by Table 2.1.

An important limiting case is the classical *continuous, constant and coherent wave*, e.g. a highly stabilized **RF** generator or an ideal **CW** laser. In that case $\langle I(t)I(t+\delta) \rangle \equiv \bar{I}^2$, there are no intensity fluctuations and

$$g^{(2)}(\delta) = 1.$$

It may sound somewhat surprising at first sight, but in a fully coherent radiation source, such as an ideal laser, the photons are distributed as randomly as possible!

Quite generally, for long delay times δ there are no correlations in the statistical intensity fluctuations and thus

$$g^{(2)}(\delta) \rightarrow 1 \quad \text{always holds for} \quad \delta \gg \tau_c.$$

2.1.6 Photon “Bunching” Experiments

The proposal of Hanbury BROWN and TWISS (1954) for “A new type of interferometer for use in radio astronomy” marks the beginning of quantum optics (GLAUBER 2006). In their pioneering investigations, correlations in the intensity of an extended light source were measured for the first time – both in a table top laboratory exper-

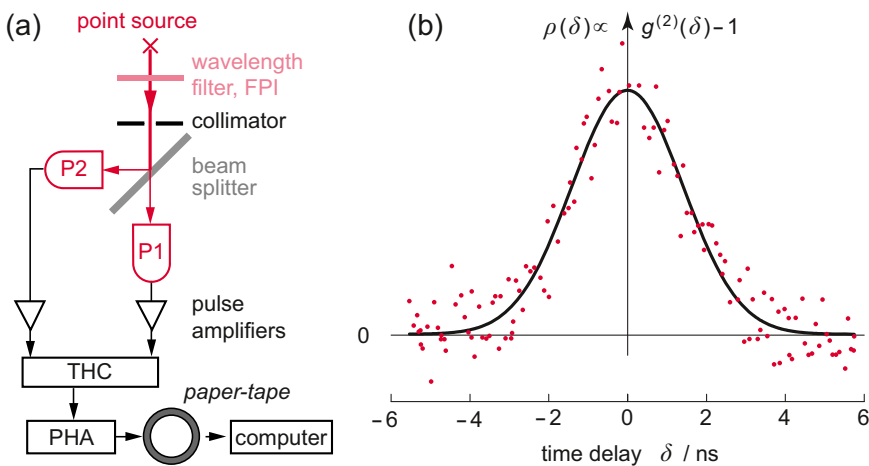


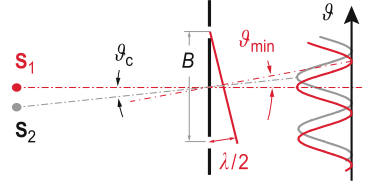
Fig. 2.6 Photon bunching experiment according to PHILLIPS et al. (1967). **(a)** Schematic of the experimental setup with two photo-multipliers P1 and P2, time to height converter (THC) and pulse height analyzer (PHA). **(b)** Observed true two photon coincidence rate (normalized) as a function of time delay between the two photons; light filtered with a 3 cm FPI; the maximum is $\rho(0) \sim 17.3\%$

iment (1956a, 1958) and for light from a star (1956b). In such an **HBT experiment** the **intensity** of chaotic light is registered by two spatially separated detectors whose signal is then correlated – in contrast to YOUNG’s double slit experiment where the **electric field amplitudes** of the light are superposed. However, before we can discuss **HBT** type experiments, we shall have to introduce spatial or lateral coherence in Sect. 2.1.7.

Conceptually somewhat more straight forward are so called photon “bunching” experiments – a number of which were performed in the years following the original **HBT** experiment. One with particular nice data by PHILLIPS et al. (1967) is sketched schematically in Fig. 2.6(a). Quasi-monochromatic light from a mercury spectral lamp passes a narrow band filter and then an **FPI** to select the 435.8 nm line and reduce the bandwidth, i.e. to increase the coherence time. The light beam is then strongly collimated by pin holes with diameters of 0.3 mm and 2 mm, separated by 1.5 m before it reaches a beam splitter which provides two branches of equal light intensity. Two separate photo-multipliers P1 and P2 are setup to detect individual, single photons, which are recorded after amplification and clipping as pulses with a rise time of less than 2 ns. The time delay between these pulses is registered by the combination of a *time to pulse height analyzer* (THC) and a *multichannel pulse height analyzer* (PHA). Data storage and communication with a computer was at that time still done by punched paper-tape.

The experiment thus determines coincidence rates for counting a photon in branch 2 after a time δ when a photon has been registered in branch 1 (or vice versa). If the individual count rate at P1 is R_1 and at P2 it is R_2 (in this experiment some 10^4 counts/s). The coincidence rate is $R_1(t) \times R_2(t + \delta) \times \Delta\delta$, in this exper-

Fig. 2.7 Interference from two sources



iment $< 10 \text{ s}^{-1}$ with $\Delta\delta$ (here some ns) being the time resolution of the electronics. One subtracts the statistical coincidence rate $\overline{R_1} \times \overline{R_2} \times \Delta\delta$ (corresponding to the coincidence rate for $\delta \rightarrow \infty$). In summary, one records the true coincidence rate, which properly normalized is

$$\rho(\delta) = \frac{R_1(t) \times R_2(t + \delta)}{\overline{R_1(t)} \times \overline{R_2(t)}} - 1 \propto g^{(2)}(\delta) - 1 = [g^{(1)}(\delta)]^2.$$

A typical result is shown in Fig. 2.6(b). The frequency bandwidth of the FABRY-PÉROT filter was in this case ca. $\Delta\nu_{1/2} \simeq 160 \text{ MHz}$, in fair agreement with 208 MHz gleaned from the correlation measurement. The maximum of the normalized true coincidence was found to be $\rho(0) \sim 17.3 \%$ – the authors attribute the fact that *it is not* $= 1$ to the finite temporal resolution of the electronics, but also to finite lateral coherence (a compromise had to be found between a reasonable count rate and low angular divergence of the beam). But clearly, the experiment shows beyond any doubt, that the probability to register two photons at the same time is significantly higher than expected by purely random coincidences (observed at long delay times) – in full agreement with the considerations outlined in Sect. 2.1.5.

2.1.7 Spatial or Lateral Coherence

So far, in our discussion of coherence experiments we have assumed strictly parallel, quasi-monochromatic light rays. (In the experiment just explained, this was approximated well enough by the high efforts to collimate the light.) Now we also give up this usually somewhat unrealistic assumption. Even laser beams have a finite angular divergence, as we have discussed in Sect. 1.2. The problem with this fact and the measurement of interference patterns is, that different incident angles lead also to a phase difference, and hence, to shifted interference fringes. Let us start with a rough estimate of this effect, before we enter into a more rigorous treatment. We consider two point like sources at very large distance. Their (quasi-monochromatic) light is assumed to be parallel and to be diffracted by a YOUNG's double slit arrangement, the slit distance being B . As sketched in Fig. 2.7, the first interference minimum from source S_1 (red fringe pattern) is found at an angle ϑ_{\min} for which $\lambda/2 \simeq B\vartheta_{\min}$. Source S_2 , which is seen under an angle ϑ_c , generates its own interference pattern (grey) with its main maximum at an angle ϑ_c . Sketched is a partial overlap for both fringe patterns. If the two sources were still further apart, so that

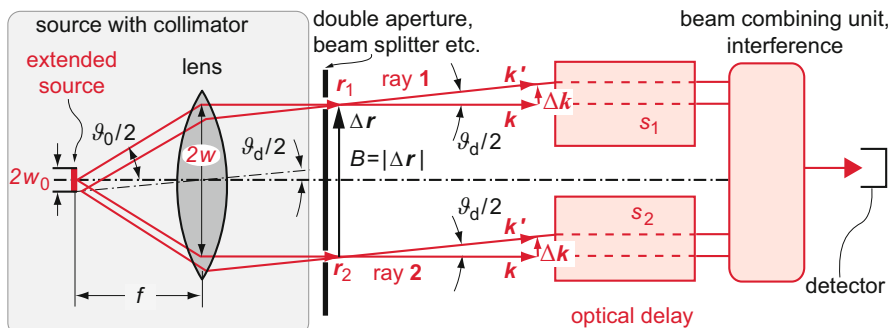


Fig. 2.8 On spatial coherence: very schematic diagram of an interference experiment with slightly diverging light rays **1** and **2** from an extended source (uniform disc angular diameter ϑ_d)

$\vartheta_c = \vartheta_{\min}$, the maximum from S_2 would fully coincide with the first minimum from S_1 : hence, the fringe patterns would disappear: interference structures can only be discerned if

$$\vartheta_c \leq \frac{\lambda}{2B}. \quad (2.44)$$

The light is said to be *spatially or laterally coherent* if ϑ_c is smaller than this limit. Even though the assumed limit is somewhat arbitrary, clearly this spatial coherence or incoherence will influence the fringe visibility discussed in Sect. 2.1.4 for temporal (or longitudinal) coherence.

To obtain a quantitative understanding we now consider an extended, stationary light source of diameter $D_0 (= 2w_0)$ which is collimated by a lens with a focal length f and a (useable) diameter $D (= 2w)$, as sketched in Fig. 2.8. The initial divergence of this “beam” is given by $\vartheta_0 \approx D_0/f$ (angular diameter), quite analogous to the situation for a Gaussian beam according to Fig. 1.16, if we identify the disc radius w_0 with the beam waist and the Gaussian divergence angle θ_e with $\vartheta_0/2$. For not too large aperture angles ϑ_0 , the (full) angular divergence ϑ_d after collimation is

$$w\vartheta_d \simeq w_0\vartheta_0, \quad (2.45)$$

if the lens is used up to a diameter $2w$. With this more realistic description of a light beam we have to modify our treatment of the interference experiment presented in Sect. 2.1.4.

The following derivation is completely independent of the origin of the two slightly divergent light rays. The source-collimator arrangement (grey shaded area in Fig. 2.8) may e.g. be replaced by a distant star that emits light with a small divergence angle ϑ_d (“uniform disc angular diameter” equivalent to its diameter divided by its distance). The light may be collected by two different mirrors or telescopes placed at a distance $B (= 2w)$. In the context of astronomical interferometry this distance is called *baseline*. We shall come back to this context in Sect. 2.1.8.

Comparison of Figs. 2.3 and 2.8 shows that we now have to treat interferences of plane waves with wave vectors \mathbf{k}_i around the mean wave vector \mathbf{k} . In analogy to the averaging over frequencies, we now have to sum in addition over the contributions from all \mathbf{k}_i . As before the contributions from superpositions belonging to different \mathbf{k}_i and \mathbf{k}_j statistically average out: as before “each photon interferes only with itself”.

The key question is now whether, and to what extent, the interference patterns from different \mathbf{k}_i disturb each other. We start again from (1.106) and write the electric fields propagating from \mathbf{r}_1 and being detected at time $t_1 = t - s_1/c$ as

$$E_i^+(\mathbf{r}_1, t_1) = \int E_i^+(\omega) e^{i(\mathbf{k}\mathbf{r}_1 - \omega t_1 + \Delta\mathbf{k}_i \cdot \mathbf{r}_1)} d\omega. \quad (2.46)$$

The propagation vectors \mathbf{k}_i of the individual wave-packets is now written with reference to the central wave vector \mathbf{k}

$$\mathbf{k}_i = \mathbf{k} + \Delta\mathbf{k}_i. \quad (2.47)$$

The interference term $I_{12} \propto \langle E_i^+(\mathbf{r}_1, t_1) E_j^-(\mathbf{r}_2, t_2) \rangle$ – after summation over different wave-packets and exploiting the “one photon interferes only with itself” rule – becomes in analogy to (2.28)

$$I_{12} = 2 \frac{C^2}{2\pi} \text{Re} \int d\omega \langle |E_i(\omega)|^2 e^{i[\mathbf{k} \cdot (\mathbf{r}_1 - \mathbf{r}_2) - \omega(t_1 - t_2) + \Delta\mathbf{k}_i \cdot (\mathbf{r}_1 - \mathbf{r}_2)]} \rangle. \quad (2.48)$$

The averaging $\langle \dots \rangle$ must include the angular divergence reflected in $\Delta\mathbf{k}_i \cdot (\mathbf{r}_1 - \mathbf{r}_2)$. We write the distance vector $\mathbf{r}_1 - \mathbf{r}_2 = \Delta\mathbf{r}$, with $|\Delta\mathbf{r}| = B$, and account for the fact that $\Delta\mathbf{r}$ is per definition perpendicular to \mathbf{k} , hence $\mathbf{k} \cdot \Delta\mathbf{r} = 0$ holds. The delay time is again given by $\delta = t_1 - t_2 = (s_1 - s_2)/c$. Thus, (2.48) becomes

$$I_{12} = 2a_1 a_2 \text{Re} \int d\omega e^{i\omega\delta} \langle \tilde{I}_i(\omega) e^{i\Delta\mathbf{k}_i \cdot \Delta\mathbf{r}} \rangle. \quad (2.49)$$

The averaging $\langle \dots \rangle$ is greatly simplified by assuming $k_i \simeq \omega_c/c = k$, i.e. keeping it constant at its average value. This is a reasonable approximation for narrow band radiation $\Delta\omega_{1/2} \ll \omega_c$, so that k does not change significantly over the spectral distribution $I(\omega)$. Then the averaging in (2.49) can be factorized.

To evaluate the angular part determined by $\exp(\Delta\mathbf{k} \cdot \Delta\mathbf{r})$, we read from Fig. 2.8 for small angular divergence ϑ_d , that the projection of $\Delta\mathbf{k}$ onto the drawing plane is essentially parallel to $\Delta\mathbf{r}$ so that

$$\Delta\mathbf{k} \cdot \Delta\mathbf{r} = |\Delta\mathbf{k}| B \cos \varphi = u \cos \varphi, \quad \text{with } u = |\Delta\mathbf{k}| B = k B \vartheta \quad (2.50)$$

representing the polar angle θ at which the light from the source enters, while φ is the azimuthal angle of $\Delta\mathbf{k}$ in respect of $\Delta\mathbf{r} = \mathbf{B}$ in a plane perpendicular to \mathbf{k} . We recall that we consider a light source with a small angular diameter ϑ_d , e.g. a collimated disc or a distant star, with an intensity distribution $I(\theta, \varphi) = I(u/kB, \varphi)$.

The averaging over the angular part in (2.49) (essentially over a cone with $0 \leq \theta \lesssim \vartheta_d/2$ or $0 \leq u \lesssim kB\vartheta_d/2$), properly normalized, may be written

$$\begin{aligned} g^{(1s)}(x) &= \text{Re}\langle e^{i\Delta\mathbf{k}_i \cdot \Delta\mathbf{r}} \rangle = \text{Re} \frac{\int u du \int_0^{2\pi} I(u/kB, \varphi) e^{iu \cos \varphi} d\varphi}{\int \int_0^{2\pi} I(u/kB, \varphi) u du d\varphi} \\ &= \text{Re} \frac{\int \int I(\xi, \eta) e^{ik(p\xi + q\eta)} d\xi d\eta}{\int \int d\xi d\eta I(\xi, \eta)}. \end{aligned} \quad (2.51)$$

In the second line, the integrals are just rewritten from cylindrical coordinates u, φ into a Cartesian $\xi \eta$ plane perpendicular to the average wave vector \mathbf{k} (for details see BORN and WOLF 2006, Chap. 10.4). In analogy to (2.29), $g^{(1s)}(x)$ is called *degree of spatial coherence* (or *spatial correlation function*), and (2.51) represents the VAN CITTERT-ZERNICKE theorem according to which the *degree of spatial coherence is equal to the normalized FOURIER transform of the intensity distribution of the source*.

We specialize now to an “uniform disc” model for the light source, with constant emission $I(u/kB, \varphi)$ for $0 \leq \theta \leq \vartheta_d/2$, independent of φ and obtain

$$g^{(1s)}(x) = \langle e^{i\Delta\mathbf{k}_i \cdot \Delta\mathbf{r}} \rangle = \frac{1}{\pi u_d^2} \int_0^x u du \int_0^{2\pi} e^{iu \cos \varphi} d\varphi. \quad (2.52)$$

The prefactor $1/\pi u_d^2$ ensures proper normalization. The double integral here is the same as that encountered in Sect. 1.2.2 where we have derived the diffraction pattern from a uniform circular aperture.⁵ With (1.66) for $n = 0$ it can be expressed by the first-order BESSEL function $J_1(x)$,

$$g^{(1s)}(x) = \frac{2J_1(x)}{x} \quad \text{with } x = kB\vartheta_d/2 = \pi\vartheta_d B/\lambda \quad (2.53)$$

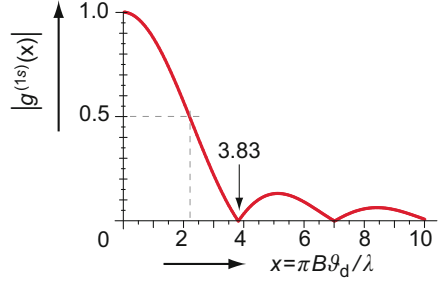
as illustrated in Fig. 2.9. For $x = 3.83$ (2.53) reaches zero and interference structures disappear: one says that the *light is laterally coherent* if

$$\frac{\pi\vartheta_d B}{\lambda} < 3.83 \quad \text{or} \quad \vartheta_d < \frac{1.22\lambda}{B}. \quad (2.54)$$

This may be compared to our initial, crude estimate (2.44) – giving the right order of magnitude. We recognize the second inequality as the famous RAYLEIGH criterium for the angular resolution of optical instruments, if we interpret B as diameter of the objective lens. One may also convert this into lateral resolution by setting $\vartheta_d = w_0/f$, where w_0 is the smallest object that can be resolved and f the focal length

⁵Note, however, that here the *diameter* B of the entrance pupil replaces the *radius* of the aperture w_0 there: essentially, (2.52) describes how the diffraction pattern from the source affects the interference patterns in the experimental scheme Fig. 2.8.

Fig. 2.9 Absolute value of the degree of spatial coherence (2.53) as a function of $x = \pi B \vartheta_d / \lambda$, with the baseline B , the angular diameter of the light source ϑ_d and wavelength λ ; note that $3.83/\pi = 1.22$ so that the first diffraction minimum is found at $\vartheta_d = 1.22\lambda/B$



of the objective. Note that for larger opening angles ϑ_d , as often encountered in optical instruments, the

$$\text{lateral coherence condition is } \sin \vartheta_d < 1.22\lambda/B.$$

The final evaluation proceeds as in Sect. 2.1.4. Thus, the overall interference patterns given by

$$I(\delta) = I_1 + I_2 + 2\sqrt{I_1 I_2} \operatorname{Re}[g^{(1)}(\delta)]g^{(1s)}(\pi \vartheta_d B / \lambda_c) \cos \omega_c \delta, \quad (2.55)$$

replacing (2.30). The *visibility* of the interference fringes (2.31) is thus determined by $|g^{(1s)}|$. For $I_1 = I_2$ we obtain at $\delta = 0$:

$$V = \frac{I_{\max} - I_{\min}}{I_{\max} + I_{\min}} = |g^{(1s)}(x)| = \left| \frac{2J_1(x)}{x} \right| \quad \text{with } x = \pi \vartheta_d B / \lambda_c. \quad (2.56)$$

We recall that our derivation is for a circular disc light source with a *uniform angular diameter* ϑ_d , such as a distant star. A systematic measurement of the visibility V as a function of baseline B at well defined wavelengths λ_c thus allows one to extract ϑ_d as will be discussed in the next subsection.

To summarize: the interference structure is lost not only for long delay times $|\delta| \gg \tau_c$ – as a consequence of an optical path difference larger than the coherence length, $|s_1 - s_2| \gg \ell_c$. It also disappears for a light beam with too large lateral extension or too large angular divergence (2.54). This can be rewritten for a light beam of a *half divergence angle* $\theta_e = \vartheta_d/2$, a radius $w = B/2$ (see Fig. 2.8) and with $3.83 \lesssim 4$:

$$w < \frac{\lambda}{\pi \theta_e} \simeq \frac{2}{\theta_e k} := w_{\text{coh}}. \quad (2.57)$$

Light is considered coherent if the left inequality holds. We have defined here (somewhat arbitrary) w_{coh} , a *spatial (lateral) coherence radius* of a light source. Correspondingly, for a source of radius w we call $\theta_e = \lambda/\pi w$ the *coherence angle*.

This description implies that all wave-packets originating from a cross section $\lesssim \pi w_{\text{coh}}^2$ are considered coherent: their respective interference patterns do not dis-

turb each other significantly. Hence,

$$A_{\text{coh}} = \pi w_{\text{coh}}^2 = \frac{\lambda^2}{\pi \theta_c^2} = \frac{\lambda^2}{\delta \Omega_c} \quad (2.58)$$

is the *coherence area of a light source*, where $\delta \Omega_c = \pi \theta_c^2$ is the solid divergence angle of the beam. Correspondingly, for a given width w of a source, we call $\delta \Omega_c = \lambda^2 / \pi w^2$ the *coherence (solid) angle*. We finally combine the lateral coherence area (2.58) with the longitudinal coherence length according to (2.20) – slightly arbitrarily and for a Lorentzian frequency distribution – and define a *coherence volume*

$$V_{\text{coh}} = A_{\text{coh}} 2\ell_c = \frac{4c\lambda^2}{\Delta\omega_{1/2}\delta\Omega_c}. \quad (2.59)$$

Photons are considered as coherent if they originate from a cylindrical volume extending from $+\ell_c$ to $-\ell_c$ in \mathbf{k} direction around the center of the beam with of radius w_{coh} (beam waist) with a solid divergence angle $\delta \Omega_c$.

For a “beam” of light derived from a chaotic (or natural) source, these considerations just imply that phase fluctuations within the so defined coherence volume are small enough so that interference structures are not disturbed significantly. For a *freely propagating, stationary laser beam* the definition of a coherence volume comes even more naturally: Let the *radial profile of the beam be Gaussian*, and the *frequency profile Lorentzian*. The lateral coherence radius is identified as the beam waist w_0 (we recall that according to Table 1.1 86 % of the total power flows through the corresponding cross section). On the other hand, the relation of w_0 to the divergence angle (1.55) is identical to that of w_{coh} according to (2.57). And the (longitudinal) coherence lengths Table 2.1 is the same as just assumed. In summary, expressions (2.57)–(2.59) also hold for a *Gaussian laser beam with a Lorentzian spectral profile*.

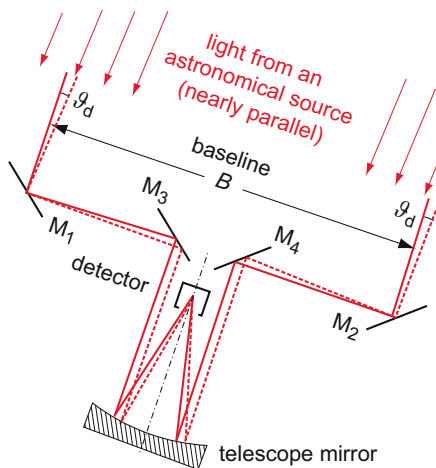
2.1.8 Astronomical Interferometry

A direct application of the concept of spatial coherence just developed, is the lateral or angular characterization of extended light sources emitting at far distances: this is exploited by astronomical interferometry which dates back to MICHELSON and PEASE (1921) who mounted a steel beam of initially 6 m length with four mirrors on top of a 2.5 m diameter telescope on mount Wilson, California, in order to determine the lateral degree of coherence of stellar light.

The scheme is sketched in Fig. 2.10. If one changes the distance B (the so called *baseline*) between the two light receiving mirrors M_1 and M_2 , according to (2.54) interference is only observable for $\vartheta_d \leq 1.22\lambda/B$. This allows one to determine the angular diameter ϑ_d at which the object studied is seen (e.g. a disc like star, double stars). If the distance of the star is known, one may thus determine its diameter.

The resolving power of such an astronomical interferometer depends on the fringe *spatial frequency* B/λ : the larger it is, the smaller divergence angles can

Fig. 2.10 Scheme of the original MICHELSON stellar interferometer



be determined. For example, for a baseline of $B = 20\text{ m}$ and observation of visible light an angular divergence of about $\theta = 0.007'' = 7\text{ mas}$ can still be resolved.⁶ MICHELSON, his coworkers and his successors determined quite a number of angular diameters in that way. Immense technical and methodological progress has been made since MICHELSON's ground breaking work, now nearly a century ago. The interested reader is referred to the excellent review by MONNIER (2003) as a starting point.

The most dramatic advances seem to have been made during the past decade – at least that's how it looks from the outside of this specialized field of research (i.e. to the authors of this textbook). A whole flock (at least a dozen with more to come) of very powerful optical/infrared interferometric arrays (as opposed to single baseline interferometers) has started operation during the past years, exploiting all advanced techniques one might dream of in this context (including adaptive optics, fast high precision optical delay lines, low noise high speed VIS and near IR detectors, highly sensitive digital imaging, advanced control and evaluation algorithms, fast computers).

Figure 2.11(a) schematically illustrates the design of modern stellar interferometers, which may be compared to the original MICHELSON setup Fig. 2.10. Key elements are the two light receiving telescopes, the beam guiding (“relay”) optics, the delay lines and the beam combining unit. Note that the effective baseline B used for interferometry is the “projected baseline” (perpendicular to the direction of the incident radiation) – as opposed to the distance between the two telescopes b .

Today, the world's largest telescopes, the two 10 m diameter KECK telescopes in Hawaii as well as the four 8.5 m telescopes at the European southern observatory in Chile (ESO) can ‘of course’ be combined to interferometric setups (the latter up to a baseline of 100 m) – even if only for rather limited observation times. Specialized sites such as CHARA on Mount Wilson provide a facility for astronomical

⁶ 1 milli-arcsecond = 1 mas = $2\pi \times 10^{-3} / (60 \times 60 \times 360) = 4.848 \times 10^{-9}\text{ rad}$.

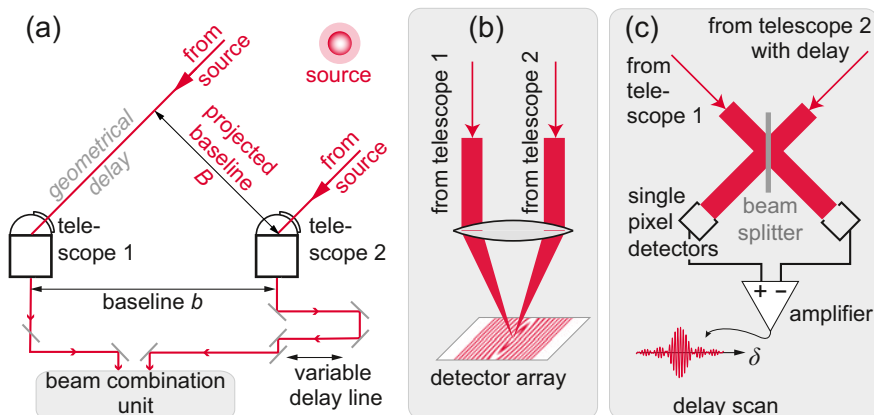


Fig. 2.11 Schematic of modern astronomical interferometers adapted from MONNIER (2003). (a) Overall layout with the telescopes, the beam guiding optics, delay line and beam combination. Two types of beam combination schemes are shown: (b) *image plane* interference (similar to YOUNG’s double slit setup), and (c) *pupil plane* where the collimated beams are brought to interference by a beam splitter

interferometry in the optical/infrared spectral range. Its 6 collecting telescopes with diameters of “only” 1 m each, are arranged in a “Y” configuration and can be combined to a total of 15 baselines, ranging from $b = 31$ to 331 m. The limiting angular resolution is specified with 0.65 mas in the NIR and 0.15 mas in the VIS – that corresponds to about the diameter of Nils Armstrong’s helmet on the moon, if directly viewed from the earth. Anyone who ever adjusted a laser system on a laboratory table may vaguely imagine the technological challenges to stabilize and manipulate an interferometer mirror setup over distances of more than 300 m with the necessary sub-wavelengths distance control and angular alignment precision! Laser metrology makes it possible.

These facilities are by now extremely productive, with measuring angular diameters of astronomical objects as well as in interferometric image reconstruction. BOYAJIAN et al. (2012) point out that 8231 stellar objects with known angular diameters were listed as of July 2004. However, of these the angular diameters for only 24 main sequence stars had been determined with an accuracy of better than 5 %, thus giving hope for quantitative modelling. Their 2012 paper alone reports angular diameters for 44 main sequence stars with a precision of better than 4 %!

Figure 2.12 illustrates typical data obtained in this work for two arbitrary examples. Plotted are the visibilities at $\lambda = 2.14 \mu\text{m}$, derived from temporal interference patterns of the type shown in Fig. 2.4 (after suitable calibration). The individual data points are measured at the 15 baselines of CHARA. Since the projected baseline B depends on the inclination of the observed star, which changes with time due to earth rotation, the number of data points is much greater than 15 and allows for sufficient precision. The data sets for each star are then fitted by functions similar to (2.56) (see Fig. 2.9). As illustrated in Fig. 2.4, quite different parts of the spatial correlation function (2.56) are exploited in these measurements, depending on the respective

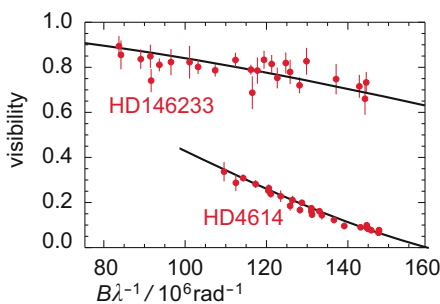


Fig. 2.12 Examples of visibilities for two stellar objects as determined by BOYAJIAN et al. (2012) at the CHARA interferometric array. The (red) data points were taken at a series of values (baseline/wavelength) = $B\lambda^{-1}$. Note that the full black curves are *not* straight lines; rather they are fits by functions essentially of the type (2.56), from which the disc diameter angle is derived: $\vartheta_{LD} = 1.623 \pm 0.004$ mas for HD4614 and $\vartheta_{LD} = 0.780 \pm 0.017$ mas for HD146233

angular diameters of the stars, here exemplified for $\vartheta_{LD} = 1.623 \pm 0.004$ mas and $\vartheta_{LD} = 0.780 \pm 0.017$ mas.⁷

We cannot close this topic without at least mentioning radio-frequency interferometry. Radio astronomy is a very powerful and highly developed area of modern astronomy, with hundreds of modern facilities worldwide, operating at wavelengths between 1.3 mm and several metres. Baselines of radio-frequency interferometers must be much larger than optical or infrared interferometers to allow detection of the same angular diameters $\vartheta_d \simeq \lambda/B$. However, radio-frequencies have the great advantage that amplitudes and phases can be recorded directly, while at optical wavelengths typically only cycle averaged intensities can be detected. Hence, amplitudes have to be superposed locally in a beam combining unit to record interference patterns.

In contrast, radio frequency interferometry correlates the amplitudes electronically, and no local superposition on the detector is needed. The signals (amplitudes and phases) may be collected anywhere in the world and be brought to “interfere” later on by a mathematical algorithm in a powerful computer.

This concept is realized in *very long baseline (radio) interferometry networks*, e.g. in the global mm-VLBI array in which several dozens of the most powerful radio telescopes of the world co-operate – including very large single dishes such as the 100 m diameter telescope at Effelsberg (Germany) and the 305 m telescope at Arecibo (Puerto Rico), as well as a number of large radio telescope arrays. All what needs to be done is to record simultaneously the electric field of a particular frequency and direction received from space, store it on a tape, and provide that with an accurate time marker – based essentially on synchronized atomic clocks (or masers). With baselines of more than 10000 km an angular resolutions of about

⁷While (2.56) is exact for a *uniform disc* (UD), astronomical models also account for *limb-darkening* (LD), which in the present case leads to a correction of about 2 %.

50 micro-arcsec can be obtained at 3 mm wavelength – which in spite of the much longer wavelengths is a factor of three better than today’s best optical resolution.

At present, the transport of data by magnetic tape is still a bottle neck. But research is underway to use fast optical networks (the next generation internet) for rapid data transfer into the central processing computer. Located anywhere in the world – it constitutes, so to say, a very flexible “beam combining unit”.

Of course, different information from space is carried by optical/infrared vs. radio-frequency emission. Thus, both types of interferometry are complementary, and progress will continue. Even space based interferometry is discussed, both for the optical and for the radio-frequency range.

2.1.9 HANBURY BROWN-TWISS Stellar Interferometer

One may determine the degree of lateral coherence also by measuring the second-order correlation function, i.e. by recording the intensity correlations and exploiting (2.41). Hanbury BROWN and TWISS have suggested for the first time such an experiment in 1954. They tested it in a laboratory setup with a spectral lamp (1956a, 1958) and performed the first successful astronomical measurement determining the angular diameter of Sirius (1956b) based on a measurement of intensity correlation.

In principle, such kind of measurement is much more flexible than the interferometry just described – one simply has to record intensities at two detectors, separated by a baseline \mathbf{B} , and to determine the correlation $g^{(2)}(\mathbf{B}) \propto \langle I(\mathbf{r}_1)I(\mathbf{r}_2) \rangle = \langle I(\mathbf{r}_1)I(\mathbf{r}_1 + \mathbf{B}) \rangle$ between these signals according to (2.36). With (2.41) one derives the first-order degree of coherence $g^{(1)}(\pi \vartheta_d B / \lambda)$, the same quantity as measured by an interferometer. But with such technique there is no need for a highly stable setup, precisely adjusted to a fraction of a wavelength over long distances, and even the telescopes do not require high quality as long as one can resolve the object studied. The baseline B can easily be varied and may, in principle, be chosen very long as the signal can be registered at widely separated locations. The setup originally used by BROWN and TWISS (1956b) is shown in Fig. 2.13(a). They actually used two standard search light mirrors of 1.56 m diameter as telescopes. The normalized second-order correlation function is recorded as a function of the projected baseline distance B . One expects a signal corresponding to Fig. 2.5, convoluted with the experimental resolution. As an example, in Fig. 2.13(b) the normalized signal $g^{(2)}(B) - 1$ is plotted for the star Sirius, which was the test object of BROWN and TWISS (1956b). From the fit shown in the graph an angular diameter of 63 mas was determined.

Hanbury BROWN continued a successful career as a radio astronomer, but still made several contributions to measuring stellar diameters based on his method in the optical spectral region. However, according to DAVIS and LOVELL (2003), “with rapid improvements in the technology of the phase-correlation interferometer, Hanbury’s intensity interferometer did not survive as a technique for the measurement of the angular sizes of radio sources. As Hanbury later remarked, he had spent two years ‘building a steamroller to crack a nut’.”

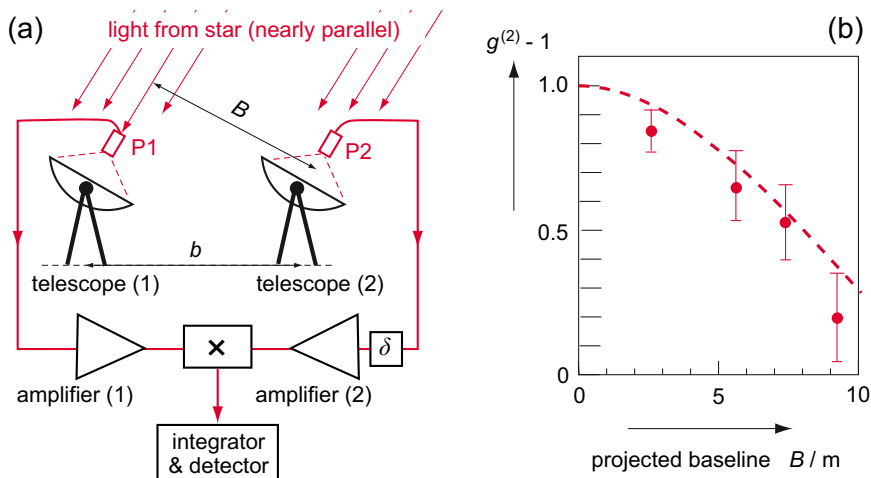


Fig. 2.13 Hanbury BROWN-TWISS stellar interferometer. **(a)** Experimental setup according to BROWN and TWISS (1956b). The two “telescopes” were standard searchlight mirrors of 1.56 m diameter and the baseline was varied up to $B \lesssim 10$ m. The detector also acts as integrator. **(b)** Comparison of experiment and theory for a measurement of the angular diameter of Sirius determining the angular diameter to be 63 mas; adapted from BROWN and TWISS (1956b)

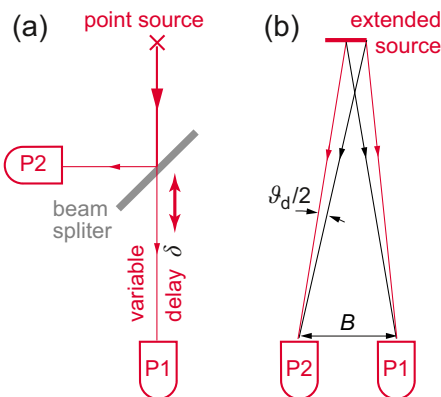


Fig. 2.14 Two varieties of the basic concept for Hanbury BROWN-TWISS type experiments. In each case the signals from the two detectors P1 and P2 are correlated (see text). **(a)** Radiation (photons or other particles) originate from a point like source with limited temporal coherence; the total flux is split into two equal branches, one of which can be delayed by a variable time δ . **(b)** The two branches originate from an extended source with limited lateral coherence, corresponding to a phase difference $\pi \vartheta_d B / \lambda$.

To fully appreciate the impact that the **HBT** concept and its realization had, as a starting point of quantum optics, let us look again at its essential ingredients. Figure 2.14(a) gives a highly simplified schematic of the photon bunching experiment (temporal/longitudinal coherence) introduced in Sect. 2.1.6. The incoming

light, *highly collimated from a point like source*, is split into two equal branches and is detected by two photo-multipliers. One records the probability for detecting one photon at detector (P1) *and* another photon at the other detector (P2) – with some time-delay δ , corresponding to a phase difference $\omega\delta$. This time delay between pairs of photons is measured electronically (see e.g. Fig. 2.6). Figure 2.14(b) shows the scheme of the original HBT experiment with an *extended light source*. It differs from (a) by the fact that now the lateral extension of the source (angular diameter ϑ_d) creates a phase difference $\pi \vartheta_d B / \lambda$ between the two detectors as explicated in Sect. 2.1.7. In this case, the baseline B is varied.

In both cases one measures the second-order correlation function (2.38). And in either case one finds (in an ideal experiment) for statistical light sources that the correlated signal at $\delta = 0$ (or at $b = 0$) is twice that for $\delta \rightarrow \infty$ (or for $b \rightarrow \infty$, respectively) – provided the detectors are sufficiently fast, i.e. their response time is much shorter than the temporal coherence time of the source (for that purpose the light is passed through a narrow band pass filter prior to detection). In contrast, a fully classical source, such as an ideal, intense CW laser beam, shows no enhanced second-order correlation at any time – the photons are distributed completely at random as we shall discuss in Sect. 2.2.

As recently pointed out by KLEPPNER (2008), the Hanbury BROWN-TWISS effect is one of those rare occasions where a classical explanation is quite straight forward, while at first sight it appears to contradict intuition from a quantum point of view: As we have seen in Sect. 2.1.7 the HBT effect arises essentially from the statistical fluctuations of the amplitudes of the radiation.⁸ Hanbury BROWN actually started as a radio engineer and was quite familiar with noisy signals. The mathematician TWISS helped him to work out the theory for his experiment on a fully classical basis.

However, from a quantum point of view the experiment was completely puzzling and started a vivid and controversial discussion: a photon is either here or there. Why should the probability of finding one simultaneously at each of the detectors ($g^{(2)}(\delta) = 2$) be higher than the statistical probability for random coincidence? But the experiment shows, even at low count rates, that if a photon is registered at (P1) the probability to register at the same time a photon at (P2) is twice that ($g^{(2)}(\delta) = 2$) for purely random arrival of completely uncorrelated beams. The answer to this puzzle is quite simple: *photons are bosons, so they may occupy the same phase space* – and in a chaotic sources they have indeed a clear tendency to bunch, rather than to occupy all modes equally. Consequently, for electrons and other fermions one may expect the opposite: *anti-bunching* as we shall see in the next subsection.

⁸We also recall that the second-order degree of coherence (autocorrelation function of the intensity) is efficiently used for measuring the duration of femtosecond pulses (Sect. 1.5). There, nonlinear processes such as SHG are applied to detect a signal which is proportional to the square of the intensity (compare Table 1.5, for $\mathcal{N} = 2$ with (2.43)). Note, however, that the results differ in the prefactor of the exponential (2 vs. 1), owing to the fully coherent nature of the laser pulse vs. the chaotic light source assumed here.

2.1.10 Bunching and Anti-Bunching

GLAUBER developed the quantum theory of light which also explains the [HBT](#) effect, consistent with the particle nature of photons (a summary of his work is available as [GLAUBER 2007](#)). But *intensity interferometry* has in the mean time successfully been adapted for other particles, exploiting the advances with fast imaging detector arrays. In high energy heavy ion and particle collisions, two particle correlations between protons, pions, or even photons again, are studied to obtain information on the “space-time geometry” of such collisions ([BAYM 1998](#)). For fermions one expects and observes anti-bunching ([HENNY et al. 1999](#); [HASSELBACH 2010](#)). Fermions cannot occupy the same phase space, they avoid each other and this can indeed be observed experimentally.

In this context it is appropriate to mention that even in photon correlations one may encounter situations where anti-bunching is observed ([KIMBLE et al. 1977](#)): if a single atom fluoresces while being excited by a not too intense radiation field, this atom will have zero probability for emitting a second photon immediately after it has just decayed from its excited state into its ground state. Even more decisive is the experiment of [GRANGIER et al. \(1986\)](#). They prepared a genuine single photon source: photons emerging from an atomic cascade are detected only when triggered by the first photon in the cascade. As expected, they observe strong anti-correlation between the triggered detection on both sides of a beam splitter. We shall come back to further experiments of this type in Chap. 10.

A relatively new field for fascinating applications of the [HBT](#) effect appears to be – quite unexpectedly – the physics of ultracold quantum gases, where complex phases and structures are revealed by such experiments. We cannot go into details here. We show, however, one particularly neat experiment on ultracold helium, which bears out the difference between fermions and bosons.

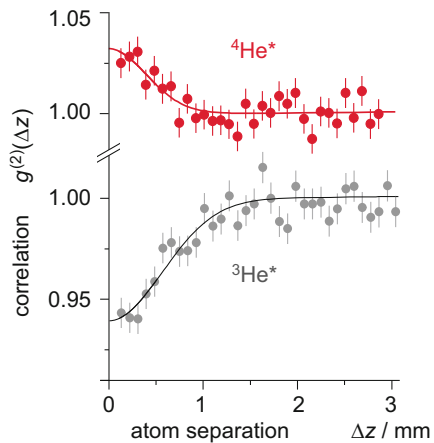
[JELTES et al. \(2007\)](#) prepared in a magnetic trap ultracold, metastable $^3\text{He}^*$ or alternatively $^4\text{He}^*$ at $0.5\,\mu\text{K}$. The trapped samples were approximately Gaussian ellipsoids of $110 \times 12 \times 12\,\mu\text{m}^3$ size. The atoms are released from the trap by turning off the magnetic field – the atoms fall under the influence of gravity and the cloud expands. They are detected by a position-sensitive detector (micro-channel plate and delay-line anode) that detects single atoms. The single atom signal simply reflects the overall shape of the (expanded) cloud.

However, the two particle coincidences allow in principle to determine a full 3D second-order correlation function $g^{(2)}(x, y, z)$ of the particle positions – analogous to the (one dimensional) schematic shown in [Fig. 2.14\(b\)](#) for photons. The best resolution is obtained in z -direction (determined by the arrival time of the atoms at the detector). The results for $g^{(2)}(0, 0, \Delta z)$ shown in [Fig. 2.15](#) give a very clear and impressive picture of anti-bunching in $^3\text{He}^*$ (fermions) and of bunching for $^4\text{He}^*$ (bosons).

Section summary

- The intensity spectrum of a light pulse is given by the (inverse) FOURIER transform of the first-order degree of temporal coherence of the field amplitude.

Fig. 2.15 Boson and fermion two particle correlation from an ultracold gas of $^3\text{He}^*$ (fermions, grey symbols) or $^4\text{He}^*$ (red symbols). If two atoms originate from the same position in space ($\Delta z = 0$), very clear anti-bunching or bunching is observed for fermions and bosons, respectively. Adapted from JELTES et al. (2007)



- With (2.16)–(2.20) we have modelled a “quasi-monochromatic”, stationary light beam. Its coherence properties are described by the first-order degree of coherence. This is summarized in Table 2.1.
- Using these classical concepts we have quantified the conditions for coherent interference of electromagnetic as observed e.g. in YOUNG’s double slit experiment. As a general rule, in quasi-monochromatic (chaotic) light *each photon interferes only with itself*.
- The [interference fringes](#) can be expressed by the first-order degree of coherence. The characteristic patterns observed as a function of time delay between the interfering beams depend on the spectral characteristic of light source. The overall [visibility](#) V contains valuable information about the lateral coherence of such a light source.
- Higher order correlation functions are defined. The (normalized) second-order degree of coherence $g^{(2)}[\delta]$ describes the correlation of field intensities at different positions in time and space. It also gives the probability to detect two photons in (delayed) coincidence. For chaotic light $g^{(2)}$ can be expressed in terms of $g^{(1)}$.
- Thus, the first-order degree of coherence can be derived from intensity correlations. This [photon bunching](#) was first observed by Hanbury BROWN and TWISS. Although classically well understood, the HBT effect is conceptually more difficult to reconcile with the particle nature of photons, and has started quantum optics in the mid 1950ies.
- Spatial (lateral) coherence complements the concept of temporal (longitudinal) coherence. [Lateral coherence is lost for extended light sources at too large divergence angles](#) since interference patterns from different parts of the source cancel each other.
- Lateral coherence is used in astronomical interferometry to determine the angular diameters of stars. Historically, the HBT effect was also exploited for this purpose. Today [powerful facilities for \(amplitude\) interferometry](#) are

used almost exclusively: arrays of interferometers in the visible and infrared spectral range, worldwide antennae networks in the radio-frequency region.

- The [HBT](#) effect can only be observed since photons are bosons. Today it is [applied successfully also to other particles](#), including fermions for which anti-bunching is observed.

2.2 Photons, Photon States, and Radiation Modes

In this section we prepare the quantization of the electromagnetic radiation field, in the following section we shall actually present the essential steps. As throughout this book, we shall do this in a heuristic manner with focus on understanding the physics – for which we may sacrifice some mathematical strictness. By no means do we intend to give a stringent introduction into quantum electrodynamics and quantum optics – for which a rich literature exists. Among the [references to this chapter](#) the ambitious reader finds several fine textbooks for further reading (LOUDON 2000; GLAUBER 2007; GRYNBERG et al. 2010; MANDEL and WOLF 1995; WEISSBLUTH 1978; MILLONI and EBERLY 2010).

Up to now, we have treated light as a completely classical radiation field. For the interaction of matter with light we have used the semiclassical approach presented in Chap. 4, Vol. 1: atoms are treated quantum mechanically, the electromagnetic field classically. For a laser beam this turns out to be a rather correct description, even though we know that light has also particle properties manifested by photons.

In fact, a laser beam contains a very large number of photons. We shall clarify in Sect. 2.2.4 what precisely that means. And we shall see, that it is this very fact which makes the semiclassical description a very good approximation. On the other hand, photon counting experiments as discussed in the previous section call for a quantum mechanical interpretation – even though a classical explanation was possible in the cases discussed so far.

For at least two reasons the introduction of a fully quantized description of the field appears to be compelling: one is *spontaneous emission* which in the semiclassical approach occurs only as a kind of afterthought and cannot really be understood. However, spontaneous emission is a key phenomenon in many areas of physics. The second reason is of a more fundamental – one might say aesthetical – nature: to document *energy conservation* for radiation induced processes. Clearly, energy is needed to excite an atom, and conversely, it cannot be lost when the atom is de-excited. The semiclassical picture does not account for this explicitly; energy comes from somewhere and gets lost to somewhere. In contrast, the fully quantized description will connect absorption and emission with the annihilation and creation of a photon, respectively, and thus expresses energy conservation explicitly.

2.2.1 Towards Quantization of the Radiation Field

Before going into details, let us get our bearings with the overall picture. Quantum mechanics, as we have used it so far, is essentially particle wave mechanics in

the SCHRÖDINGER picture. Historically, particles (electrons, atoms, nuclei) existed a long time before the invention of SCHRÖDINGER, DIRAC or KLEIN-GORDON equations. With photons, the situation is exactly opposite: the wave equation for photons, i.e. for electromagnetic radiation (based on MAXWELL's equations) existed a long time before the photon was discovered (or should we say, was “invented” as a concept?). Thus, we know the wave equation for photons already. What is required at this point is a genuine quantization of the field. We have to find a common framework for describing the states of electrons and those of photons – and their interaction. There is, however, one major difference between electrons and photons: while the former are fermions the latter are bosons. For electrons the PAULI principle holds and any state can only be occupied by one electron. In contrast, many photons can, in principle, occupy any given photon state.

Thus, the programme is as follows: We first recall the basic properties of photons and introduce the concept of *photon states*. Secondly, we take a more detailed look at the photon wave functions, called *modes of the electromagnetic field*. Thirdly, we introduce a convenient scheme of book-keeping for photons, called *second quantization*, which characterizes photon states by their occupation numbers.⁹ In the usual SCHRÖDINGER picture the *electromagnetic field* itself (as an observable) is then represented by a *time independent operator*, all time dependence will be cast into the evolution of the photon states.

We begin by recalling the well known experimental facts about photons. From the photoelectric effect we know that the energy in the electromagnetic fields is quantized in well defined packets of

$$W_{\text{ph}} = \hbar\omega, \quad (2.60)$$

associated with the particle photon. The photon travels (in vacuum) with the speed of light c and has no rest mass. We may attribute to it a relativistic mass $m_{\text{ph}} = \hbar\omega/c^2$. The momentum of the photon, also known from experiment (COMPTON effect) is

$$\mathbf{p}_{\text{ph}} = \hbar\mathbf{k} \quad \text{with} \quad p_{\text{ph}} = \frac{h}{\lambda} = \hbar\bar{\nu}. \quad (2.61)$$

Finally, photons have an intrinsic angular momentum, the *photon spin* \mathbf{S} , with a spin quantum number $S = 1$. This too is based on experimental evidence (BETH 1936), as reported in Sect. 4.1.4, Vol. 1.

Photon states $|\mathbf{k}, \mathbf{e}\rangle$ may be characterized by the photon's propagation vector \mathbf{k} and its polarization \mathbf{e} according to Sect. 1.3. One may introduce a photon spin operator $\hat{\mathbf{S}}$ and its components, in particular \hat{S}_z and express the photon states in the helicity basis $|\mathbf{e}_q\rangle$, where the z -axis is chosen parallel to \mathbf{k} . The states $|\mathbf{e}_{\pm}\rangle$ refer to circularly polarized light, and the usual angular momentum algebra applies:

$$\hat{\mathbf{S}}^2|\mathbf{e}_q\rangle = \hbar^2 S(S+1)|\mathbf{e}_q\rangle \quad \text{with} \quad S = 1, \quad (2.62)$$

⁹Actually, a similar scheme can be applied to the electronic states of atoms. But that scheme is much simpler since these states can only be occupied or not be occupied.

$$\widehat{S}_z |e_q\rangle = q\hbar |e_q\rangle \quad \text{with } q = \pm 1 \quad \text{and} \quad (2.63)$$

$$\langle e_q | e_{q'} \rangle = \delta_{qq'}. \quad (2.64)$$

Alternatively, we may use basis states for linearly polarized photons,

$$|e_x\rangle = -\frac{1}{\sqrt{2}}[|e_{+1}\rangle - |e_{-1}\rangle] \quad \text{and} \quad |e_y\rangle = \frac{i}{\sqrt{2}}[|e_{+1}\rangle + |e_{-1}\rangle], \quad (2.65)$$

following (4.7) in Vol. 1. With (2.63) one verifies that these linearly polarized states are eigenstates of \widehat{S}_z^2 :

$$\widehat{S}_z^2 |e_x\rangle = \hbar^2 |e_x\rangle \quad \text{and} \quad \widehat{S}_z^2 |e_y\rangle = \hbar^2 |e_y\rangle \quad (2.66)$$

but not of \widehat{S}_z . Rather, the expectation value of \widehat{S}_z becomes zero for the $|e_x\rangle$ as well as for the $|e_y\rangle$ state. This too is confirmed by experiment. And in complete analogy to (1.85), the most general, elliptically polarized photon may be represented by

$$|e\rangle = e^{-i\delta} \cos \beta |e_{+1}\rangle - e^{i\delta} \sin \beta |e_{-1}\rangle. \quad (2.67)$$

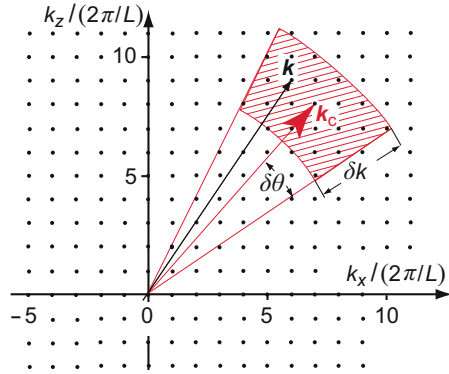
We emphasize that (2.63) includes only two states, with $q = \pm 1$, i.e. angular momentum components $\pm\hbar$ in z -direction. Even though in conventional angular momentum algebra (2.62) and (2.63) would formally define three substates (with $q = 0, \pm 1$), the particle “photon” exists only with the two angular projections, $q = \pm 1$. This somewhat unusual behaviour reflects the transverse nature of the polarization of light and the fact that photons do not have a rest mass, i.e. always propagate with the speed of light. Classically we had associated the spherical basis vectors with three oscillators: two of them oscillating in the xy plane ($q = \pm 1$) while the third oscillates along the z -axis. The corresponding radiation characteristics are described in Chap. 4, Vol. 1. Somewhat loosely one might say that the photon state with $q = 0$ does not propagate along the z -axis.

2.2.2 Modes of the Radiation Field

The photon states $|\mathbf{k}, e_q\rangle$ discussed above correspond to a single photon with polarization e_q , wave vector \mathbf{k} , and frequency $\omega = k/c$. A realistic light beam consists of many photons and a range of wave vectors. As a complete basis set for constructing any “photon wave function” one could e.g. take all plane waves with all possible values of \mathbf{k} – as we have already shown in the previous Sect. 2.1. A quasi-monochromatic, stationary light beam with a mean wave vector \mathbf{k}_c would contain a narrow range of angular frequencies $\delta\omega$ around ω_c (or $\delta k = \delta\omega/c$ around the magnitude of the wave vector k_c) and have an angular distribution of wave vectors in an angular range $\delta\theta$ (or solid angle $\delta\Omega = \pi\delta\theta^2$, respectively).

Of course, photons are in principle unbound particles, so that we would have to deal with an infinite number of basis states and an infinite number of energies. To avoid these complications, one usually switches to a very large but finite normalization volume (in real position space), say a cubic cavity of edge length L , and

Fig. 2.16 Two dimensional cut through \mathbf{k} space, divided into a grid of unit length $2\pi/L$. A light beam is characterized by the probability to find a certain wave vector \mathbf{k}_i around the mean wave vector \mathbf{k} , and by the number of photons populating this cell



perfectly conducting walls where the electric field must vanish. Mathematically this is equivalent to introducing *periodic boundary conditions*¹⁰

$$k_x = m_x \frac{2\pi}{L}, \quad k_y = m_y \frac{2\pi}{L}, \quad k_z = m_z \frac{2\pi}{L} \quad (2.68)$$

with $m_x, m_y, m_z = 0, 1, 2, 3, \dots$

Thus, a countable number of bound states emerges, called *modes of the radiation field*, to each of which we attribute a photon state $|\mathbf{k}, \mathbf{e}\rangle$.

The whole \mathbf{k} space is thus divided into very small but finite cells as sketched in Fig. 2.16. The size of the cells is determined by $\Delta k_x = \Delta k_y = \Delta k_z = 2\pi/L$, so that

$$\Delta^3 \mathbf{k} = \Delta k_x \Delta k_y \Delta k_z = \left(\frac{2\pi}{L} \right)^3. \quad (2.69)$$

Only a finite number of these modes is needed to describe a quasi-monochromatic light beam with an average wave vector \mathbf{k}_c – as indicated by the red dashed area in Fig. 2.16. Each mode is characterized by its wave vector \mathbf{k} (and polarization) and may be occupied by any number of photons.

We note an *important consequence* of this structure of \mathbf{k} space. With $\mathbf{p} = \hbar \mathbf{k}$ we may write

$$\Delta^3 \mathbf{k} = \frac{\Delta^3 \mathbf{p}}{\hbar^3} \frac{L^3}{L^3} = \left(\frac{2\pi}{L} \right)^3 \frac{\Delta^3 \mathbf{p} L^3}{h^3}. \quad (2.70)$$

Obviously (2.69) and (2.70) can only hold simultaneously if the size of

$$\text{a unit cell in phase space is } \Delta^3 \mathbf{p} L^3 = h^3. \quad (2.71)$$

¹⁰The treatment given here is quite analogue to that for electrons in a 3D box, presented in Sect. 2.4.2, Vol. 1 – except that there fermions (spin 1/2) were described and each cell in \mathbf{k} space was only filled by at most two electrons (of opposite spin).

It is important to point out here that in the preceding paragraph one key assumption has been made which is crucial (albeit plausible) for the following considerations: periodic boundary conditions in \mathbf{k} space (2.68) for the electromagnetic field. – One may, of course, also turn the arguments around and define (2.71) as the fundamental theorem: the minimal cell size in phase space is h^3 . This, together with the well defined energy $\hbar\omega$ of a photon, may be seen as the key paradigm beyond the quantization of the electromagnetic wave field. It will turn out to have decisive consequences, e.g. in the context of spontaneous emission.

We note that the size of the box, L^3 , which is our reference volume, does not necessarily refer to a real physical situation. Usually it is just a mathematical construct introduced to avoid an infinite number of photon states with which one would otherwise have to deal, and one simply has to choose L just large enough so that the grid is sufficiently fine for describing the properties of the radiation field applied.

On the other hand, there are situations where the normalization volume really refers to a genuine physical geometry, e.g. to a laser resonator or any type of optical cavity in which light may be confined. The genuine modes of this cavity will have to be used if one wants to describe an experimental situation quantitatively. Laser theory is one such application. Another field is the so called “cavity QED” which we shall touch briefly in Sect. 2.3.7. If the size of the cavity becomes comparable to the wavelength of the radiation studied one finds that even spontaneous emission is substantially modified.

Later on we shall need an expression for the *number of modes in a specified range of \mathbf{k} vectors with a given polarization*. This can now easily be derived. The number of modes $dm_{\mathbf{k}\mathbf{e}}$ between $\mathbf{k} = (k_x, k_y, k_z)$ and $\mathbf{k} + d\mathbf{k} = (k_x + dk_x, k_y + dk_y, k_z + dk_z)$ is obtained by dividing the volume element in \mathbf{k} space $dk_x dk_y dk_z$ by the size of the unit cell (2.71):

$$dm_{\mathbf{k}\mathbf{e}} = \frac{dk_x dk_y dk_z}{(2\pi/L)^3} = \frac{L^3}{(2\pi)^3} k^2 dk d\Omega = \rho(\mathbf{k}, \mathbf{e}) dk d\Omega. \quad (2.72)$$

With $\omega = kc$ we may also refer this to the angular frequency interval $d\omega$:

$$dm_{\omega\mathbf{e}} = \frac{L^3}{(2\pi c)^3} \omega^2 d\omega d\Omega = \rho(\omega, \mathbf{e}) d\omega d\Omega. \quad (2.73)$$

The values $dm_{\mathbf{k}\mathbf{e}}$ and $dm_{\omega\mathbf{e}}$ give the number of modes with polarization \mathbf{e} propagating into a solid angle $d\Omega_k$ and with wave vectors between k and $k + dk$, or angular frequencies between ω and $\omega + d\omega$, respectively. The expressions

$$\rho(\mathbf{k}, \mathbf{e}) = \frac{dm_{\mathbf{k}\mathbf{e}}}{dk d\Omega} = L^3 \frac{k^2}{(2\pi)^3}, \quad (2.74)$$

$$\rho(\omega, \mathbf{e}) = \frac{dm_{\omega\mathbf{e}}}{d\omega d\Omega} = L^3 \frac{\omega^2}{(2\pi c)^3}, \quad \text{and} \quad (2.75)$$

$$\rho(\nu, \mathbf{e}) = \frac{dm_{\nu\mathbf{e}}}{d\nu d\Omega} = L^3 \frac{\nu^2}{c^3} \quad (2.76)$$

are called *mode density*. The mode density obviously *depends on the square of the wavenumber or frequency*.

After having identified the radiation field as a discrete and countable set of modes, as a final step one extends the normalization volume L^3 to values so large (essentially to infinite) that the usual continuous spectrum is effectively recovered, i.e. L is chosen large enough to obtain a sufficiently fine mesh $\Delta k_{x,y,z} = 2\pi/L$ in \mathbf{k} space to describe the problem at hand to any degree of accuracy needed. This allows one to finally replace all necessary summations over spectral modes by an integration over the solid angle Ω and k (or ω). With the mode densities (2.74) and (2.75) just derived we may thus write symbolically

$$\sum_{\mathbf{k}} \dots \rightarrow \frac{L^3}{(2\pi)^3} \int_{k,\Omega} \dots k^2 dk d\Omega = \frac{L^3}{(2\pi c)^3} \int_{k,\Omega} \dots \omega^2 d\omega d\Omega. \quad (2.77)$$

As far as the *radiation field is spatially isotropic* one may carry out the angular integration and obtains

$$\sum_{\mathbf{k}} \dots \rightarrow \frac{L^3}{2\pi^2} \int_k \dots k^2 dk = \frac{L^3}{2\pi^2 c^3} \int_{\omega} \dots \omega^2 d\omega \quad (2.78)$$

for each specified polarization \mathbf{e} . If one investigates optical transitions induced by a well collimated radiation source, such as a laser beam, typically (2.78) cannot be used and (2.77) must be applied. We have already mentioned this aspect in our semiclassical treatment of light induced transitions in Chap. 4, Vol. 1.

Note that the mode density derived here is proportional to the normalization volume L^3 . Fortunately, as we shall see below, all measurable properties which we shall compute are densities of some kind, i.e. have to be evaluated per volume. Thus, L^3 will drop out of the final results.

2.2.3 Density of States and Black Body Radiation

We take here a little detour back to *black body radiation*. Dividing $\rho(\nu, \mathbf{e})$ given in (2.74) by L^3 , and multiplying it by 8π (integration over the full solid angle and summation over the two polarization directions) leads to the *density of states* (per volume) as introduced in Sect. 1.3.4, Vol. 1. For photons one usually refers to frequency space:

$$g(\nu) d\nu = \frac{8\pi}{c^3} \nu^2 d\nu. \quad (2.79)$$

Inserting this into the BOSE-EINSTEIN distribution (1.63), Vol. 1 for a black body radiator in thermal equilibrium, we obtain the *spectral photon density*:

$$\tilde{N}(\nu) d\nu = \frac{8\pi \nu^2}{c^3} \frac{d\nu}{\exp(h\nu/k_B T) - 1}. \quad (2.80)$$

The [chemical-potential](#) of the massless particle photon has been set here $\bar{m}_e = 0$ – it takes no energy to split or unite photons in statistical interactions (e.g. with the surrounding walls) as long as the total energy remains constant. Note that the ν^2 factor in the nominator prevents divergence for $h\nu \rightarrow 0$ (i.e. avoids the so called infrared catastrophe). Integration of (2.80) over all (positive) frequencies gives a finite value for the photon density in the black body, $N = 16(k_B T)^3 \pi \zeta(3)/(hc)^3$, with the RIEMANN function $\zeta(x)$. N amounts to about 20 photons/cm³ at 1 K. We recall now that PLANCK’s *law* describes the spectral energy density of the photons, i.e. it is obtained from (2.80) by multiplication with the photon energy $h\nu$. Comparison with (1.81), Vol. 1 shows that we have indeed derived PLANCK’s *law*.

2.2.4 Number of Photons per Mode

We still have to establish a quantitative relation between the number of photons in a specific mode and the intensity I of the electromagnetic field – or its electric field strengths E . The photon states $|e\rangle$ discussed above refer to a single photon in a specific mode k, e . In reality, however, a light source such as a laser beam, is characterized by many photons per mode. How is that number of “photons per mode” determined?

Let us start with the total number of *all photons* \mathcal{N}_e with polarization e in the normalization volume L^3 – assuming it is completely filled with radiation of intensity $I = cu$ at a photon energy $\hbar\omega$:

$$\mathcal{N}_e = u \frac{L^3}{\hbar\omega} = \frac{I}{c} \frac{L^3}{\hbar\omega}. \quad (2.81)$$

More specific, in an interval ω to $\omega + d\omega$ of angular frequencies we find

$$\mathcal{N}_e(\omega)d\omega = \tilde{u}(\omega) \frac{L^3}{\hbar\omega} d\omega = \frac{\tilde{I}(\omega)}{c} \frac{L^3}{\hbar\omega} d\omega \quad (2.82)$$

photons, with $\tilde{u}(\omega) = \tilde{I}(\omega)/c$ being the spectral radiation density and $\tilde{I}(\omega)$ intensity spectrum (per unit angular frequency). Considering the finite divergence angle $\delta\Omega$ of a light beam, the number of photons with polarization e in a frequency interval $d\omega$ per solid angle $d\Omega$ is

$$\mathcal{N}(\omega, \Omega; e) d\omega d\Omega = \frac{\tilde{I}(\omega)}{\delta\Omega} \frac{L^3}{c\hbar\omega} d\omega d\Omega. \quad (2.83)$$

Finally, we recall $dm_{\omega e}$, the number of modes (2.73) in a range $d\omega d\Omega$ of frequencies and solid angles. With this we obtain the *number of photons per mode*:

$$\mathcal{N}_{ke} = \frac{\mathcal{N}(\omega, \Omega; e) d\omega d\Omega}{dm_{\omega, e}} = \frac{\tilde{I}(\omega)}{\hbar\omega c \delta\Omega} \frac{(2\pi c)^3}{\omega^2} = \frac{\tilde{I}(\omega)}{\delta\Omega} \frac{\lambda^3}{c\hbar}. \quad (2.84)$$

We thus have worked out a relation between the *quantum mechanically relevant number of photons per mode* and the *measurable intensity per solid angle and angular frequency*. To be even more specific: with (2.21) for the maximum $\tilde{I}(\omega_c)$ of a Lorentzian spectral distribution (FWHM = $\Delta\omega_{1/2} = 2/\tau_c$) we obtain

$$\mathcal{N}_{ke} = \frac{2I}{\Delta\omega_{1/2}\delta\Omega} \frac{\lambda^3}{\pi c\hbar} = \frac{I}{\hbar\omega\delta\Omega} 2\tau_c\lambda^2. \quad (2.85)$$

As expected, \mathcal{N}_{ke} is independent of the normalization volume (both the number of photons and the mode density grow linearly with L^3). But it is proportional to the coherence time and inversely proportional to the divergence angle $\delta\Omega$ of the light source.

It is instructive to look at some numbers \mathcal{N}_{ke} for some typical light sources. Let us, e.g. take an ideal laser beam with a Gaussian radial profile and a Lorentzian spectrum. In this case, the divergence angle of the source is diffraction limited, i.e. $\delta\Omega = \delta\Omega_e$ and with (2.59) we identify the coherence volume V_{coh} . Thus, *for a diffraction limited beam* we can write

$$\mathcal{N}_{ke} = \frac{I}{c\hbar\omega} V_{\text{coh}}. \quad (2.86)$$

As $I/(c\hbar\omega)$ is the photon number density, this relation can be read as: the *number \mathcal{N}_{ke} of photons per mode is equivalent the number of photons in the coherence volume of the beam*. We recall: for a laser beam V_{coh} is simply its geometrical waist cross section πw^2 (at $1/e^2$ width) multiplied by $2\ell_c = 2c\tau_c$.

A slightly different situation is encountered for a *chaotic radiation source*. Let it have a small but finite diameter $d = 2w$ and radiate with a total power P isotropically into the full solid angle $\delta\Omega = 4\pi$. Coherent emission from its effective area πw^2 occurs into a solid angle $\delta\Omega_e = \pi\theta_e^2 = \lambda^2/\pi w^2$, with an intensity $I = P/\pi w^2$. Thus, (2.85) may be written

$$\mathcal{N}_{ke} = \frac{P}{\pi w^2 \hbar\omega} \frac{4\lambda^2}{\Delta\omega_{1/2} 4\pi} = \frac{P}{\hbar\omega} \frac{\delta\Omega_e}{4\pi} 2\tau_c.$$

The second equality states that the *number of photons per mode is equivalent to the number of photons emitted coherently (i.e. into a solid angle $\delta\Omega_e$) during twice the coherence time*.

Table 2.2 summarizes characteristic parameters for some typical radiation sources: total power, lateral extension, wavelength, bandwidth and relative bandwidth. From these one calculates coherence (half) angle, coherence time and coherence lengths according to Table 2.1 as well as the rate of coherent photon emission $P_{\text{coh}}/\hbar\omega$ and the number of photons per mode \mathcal{N}_{ke} according to (2.85).

Among the sources compared are two essentially chaotic ones (spectral lamp and atoms at rest) and three quasi-monochromatic sources with rather long coherence times. The “spectral lamp” could be a typical, commercially available device, here

Table 2.2 Characteristic parameters of five typical light sources: Total power of emitted light P , beam waist or source radius w , wavelength λ , **FWHM** of the spectral distribution $\delta\lambda_{1/2}$ and $\delta\nu_{1/2}$, coherence (half) angle $\delta\theta_c$, coherence time τ_c , coherence length ℓ_c , coherently emitted photon rate $P_{\text{coh}}/\hbar\omega$, number of photons per mode \mathcal{N}_{ke}

Source	P/W light (total)	w/mm	λ	$\Delta\lambda/\text{nm}$	$\Delta\nu_{1/2}$	$\Delta\nu_{1/2}/\nu$ $= \Delta\lambda/\lambda$
spectral lamp	0.5	5	590 nm	10^{-3}	860 MHz	1.7×10^{-6}
atoms at rest	10^{-6}	0.05	780 nm	1.2×10^{-5}	5.9 MHz	1.5×10^{-8}
CW dye laser	1	0.5	590 nm	1.2×10^{-6}	1 MHz	2×10^{-9}
TiSa laser pulse	2.0×10^{10}	0.1	800 nm	19	8.8×10^3 GHz	2.3×10^{-2}
microwave oscillator	10^3	100	3 cm	0.3	100 Hz	1×10^{-8}

derived from the above parameters:

Source	$\delta\theta_c/\text{rad}$ $= \lambda/\pi w$	τ_c/s^{-1} $= 1/\pi \Delta\nu_{1/2}$	ℓ_c/m $= c \times \tau_c$	$P_{\text{coh}}/\hbar\omega \text{ s}^{-1}$ Photons/s	\mathcal{N}_{ke}
spectral lamp	3.8×10^{-5}	3.7×10^{-10}	0.11	5.3×10^8	0.4
atoms at rest	5×10^{-3}	5.4×10^{-8}	16	2.3×10^7	2.5
CW dye laser	3.8×10^{-4}	3.8×10^{-7}	95	3×10^{18}	1.9×10^{12}
TiSa laser pulse	2.6×10^{-3}	3.6×10^{-14}	1×10^{-5}	8×10^{28}	5.8×10^{15}
microwave oscillator	0.1	3.2×10^{-3}	10^6	1.5×10^{26}	10^{24}

emitting at the Na wavelength. The “atoms at rest” might e.g. be a BOSE-EINSTEIN condensate, assuming 10^5 excited ^{87}Rb atoms to emit at the 780 nm, with the natural width of this resonance line. These two sources are assumed to emit isotropically into the full solid angle 4π . The (half) angle θ_c indicates the maximum angle within which the light can be considered as coherent. The other sources are highly directional and are assumed spatially coherent over their full cross section. The dye laser is operating **CW** in the yellow spectral range, with reasonable stabilization and a bandwidth as often used in spectroscopy. The pulsed source (ca. 1 mJ with a temporal **FWHM** of 50 fs at 800 nm) represents a standard femtosecond Titanium-sapphire laser setup, with a beam focused moderately to $w = 100 \mu\text{m}$. We assume the whole pulse to represent one mode of radiation – due to the short pulse duration with a rather broad bandwidth. Finally, we also compare with a classical radiation source, a microwave oscillator.

The characteristic quantity \mathcal{N}_{ke} derived here, the number of photons per mode, gives of course an average value if many modes are needed to describe the spectrum and the angular profile of a source. Note that these sources represent rather different types of radiation: For the spectral lamp \mathcal{N}_{ke} is very small so that most modes do not contain any photon at all; the atomic source shows already a significant probability to find one or even more photons per mode; the highly coherent laser sources as well as the microwave source contain a very large number of photons per mode, and the field can be considered as essentially classic.

2.2.5 The Multi-Mode Field and Energy

We may now explicitly write down the field variables of a multi-mode electromagnetic radiation field, i.e. its vector potential $\mathbf{A}(\mathbf{r}, t)$, and its electric $\mathbf{E}(\mathbf{r}, t)$ and magnetic field $\mathbf{B}(\mathbf{r}, t)$. They are related to each other as described in Appendix H.1.1, Vol. 1. We focus again on the electric field vector. Following (1.35) we write now

$$\mathbf{E}(\mathbf{r}, t) = \frac{i}{2} \sum_{kq} \{ \mathbf{e}_q E_{kq}^-(t) e^{i\mathbf{k}\mathbf{r}} - \mathbf{e}_q^* E_{kq}^+(t) e^{-i\mathbf{k}\mathbf{r}} \} \quad (2.87)$$

$$\text{with } E_{kq}^-(t) = E_{kq}^- e^{-i\omega t} \text{ and } E_{kq}^+(t) = E_{kq}^+ e^{i\omega_k t}. \quad (2.88)$$

The summation has to be carried out over all occupied field modes. In a classical description E_{kq} is the field amplitude in each mode, with wave vector \mathbf{k} and polarization q . As discussed previously, random phase fluctuations will have to be included if one wants to describe a stationary light beam.

We now have to make the translation to quantum mechanics, i.e. we are looking for the field operator. A good starting point is the total energy W stored in the electromagnetic field. By inserting (2.87) into (1.86) we obtain the intensity I and the energy density $u = I/c$. Integration over the whole normalization volume L^3 eventually leads to

$$W = L^3 \varepsilon_0 c |\mathbf{E}(\mathbf{r}, t)|^2 \quad (2.89)$$

$$= L^3 \frac{\varepsilon_0}{2} \sum_{kq} E_{kq}^-(t) E_{kq}^+(t) = L^3 \frac{\varepsilon_0}{2} \sum_{kq} E_{kq}^- E_{kq}^+. \quad (2.90)$$

This convincingly clear result is essentially a consequence of the confinement to a large normalization volume with periodic boundary conditions: squaring (2.87) leads to a double sum over $\mathbf{k}q$ and $\mathbf{k}'q'$. However, with integration over L^3 one finds that exponential terms of the type $\exp[i(\mathbf{k} - \mathbf{k}')\mathbf{r}]$ lead to delta functions, so that only contributions from terms diagonal in \mathbf{k} remain. Finally, with (2.88) the time dependence also drops out.

Section summary

- In this section several conceptual steps were taken to familiarize ourselves with the notion of photon states, and to prepare the quantization of the electromagnetic field.
- After recalling the quantum properties of photons, we introduced modes of an electromagnetic field by assuming a large but finite normalization volume L^3 and demanding [periodic boundary conditions](#). As a consequence we find that $\Delta^3 \mathbf{p} L^3 = h^3$ is the smallest size of a phase space cell.

- This concept allowed us to specify the **number of modes**, respectively to determine the density of modes in \mathbf{k} space.
- An important quantity which connects the classical view of a continuous electromagnetic field and the quantum description of photons is the (average) number of photons $\mathcal{N}_{\mathbf{k}e}$ per mode with a specified wave vector \mathbf{k} and polarization e . Quantitatively, $\mathcal{N}_{\mathbf{k}e}$ is related by (2.85) with intensity of the radiation, its frequency spectrum, and its angular divergence.
- For several characteristic radiation sources Table 2.2 summarizes the relevant parameters, coherence properties and numbers of photons per mode.
- Finally, we have – for the general case of a quasi-monochromatic light source with finite divergence angle – rewritten the **electric field vector** and the **energy contained in the radiation field**, using the language of field modes introduced here.

2.3 Field Quantization and Optical Transitions

2.3.1 Second Quantization and Photon Number States

So far we have not really quantized the field yet. In order to do so, one needs some quantum mechanical tools: the matrix formulation of the harmonic oscillator and second quantization. The latter is a clever method of book keeping for the population of states with particles – here of photon states with photons.

We start with the total energy (2.89) of the electromagnetic field, and consider one single mode \mathbf{k}, q populated. The field energy in this mode is

$$W_{\mathbf{k}q} = L^3 \frac{\varepsilon_0}{2} E_{\mathbf{k}q}^-(t) E_{\mathbf{k}q}^+(t) = L^3 \frac{\varepsilon_0}{2} E_{\mathbf{k}q}^- E_{\mathbf{k}q}^+ \quad \text{with } E_{\mathbf{k}q}^+(t) = E_{\mathbf{k}q}^+ e^{i\omega_{\mathbf{k}q} t}. \quad (2.91)$$

In the following we drop the indices $\mathbf{k}q$ for simplicity of writing, and introduce new variables:

$$Q = \frac{\sqrt{L^3 \varepsilon_0}}{2\omega} [E^-(t) + E^+(t)] \quad \text{and} \quad P = -i \frac{\sqrt{L^3 \varepsilon_0}}{2} [E^-(t) - E^+(t)]. \quad (2.92)$$

The inverse relations are

$$E^-(t) = \sqrt{\frac{1}{L^3 \varepsilon_0}} (\omega Q + iP) \quad \text{and} \quad E^+(t) = \sqrt{\frac{1}{L^3 \varepsilon_0}} (\omega Q - iP). \quad (2.93)$$

With this the total energy (2.91) is written as

$$W = \frac{1}{2} (P^2 + \omega^2 Q^2). \quad (2.94)$$

This expression looks very familiar: it is mathematically identical to the energy of the harmonic oscillator in classical mechanics:

$$W = \frac{p_x^2}{2m} + \frac{m\omega^2}{2}x^2.$$

The key idea is now, to identify the oscillations of the electromagnetic radiation field with the harmonic oscillator, and use the rules sketched in Chap. 2, Vol. 1 to translate the field modes into quantum mechanics. For this, Q and P must be canonical conjugate coordinates. With (2.92) we find

$$\dot{P} = -\omega^2 Q \quad \text{and} \quad \dot{Q} = P,$$

and the partial derivatives of the energy (2.94) are

$$\frac{\partial W}{\partial Q} = \omega^2 Q = -\dot{P} \quad \text{and} \quad \frac{\partial W}{\partial P} = P = \dot{Q}.$$

This set of equations are the classical HAMILTON equations in one dimension with Q and P being indeed canonical conjugates. Thus, $W := H$ represents the Hamiltonian of the electromagnetic field!

What follows is the *decisive step in the quantization process*: canonical conjugates are replaced by operators which obey the commutation rule

$$[\hat{Q}, \hat{P}] = i\hbar. \quad (2.95)$$

We now rewrite the relations (2.93) in dimensionless form by multiplying them with $\sqrt{L^3 \epsilon_0 / (2\hbar\omega)}$:

$$\hat{a} = \frac{1}{\sqrt{2\hbar\omega}}(\omega\hat{Q} + i\hat{P}) \quad \text{and} \quad \hat{a}^+ = \frac{1}{\sqrt{2\hbar\omega}}(\omega\hat{Q} - i\hat{P}). \quad (2.96)$$

With (2.95) one verifies that these operators obey the simple commutation rule

$$[\hat{a}, \hat{a}^+] = \hat{a}\hat{a}^+ - \hat{a}^+\hat{a} = 1, \quad (2.97)$$

which may be recast into

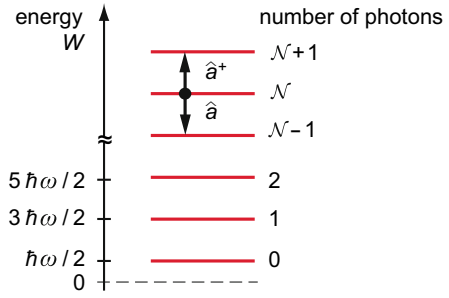
$$\hat{a}\hat{a}^+ = \hat{a}^+\hat{a} + 1 = \hat{N} + 1. \quad (2.98)$$

Here we have introduced the so called *number operator*

$$\hat{N} = \hat{a}^+\hat{a}. \quad (2.99)$$

The Hamiltonian of the electromagnetic field (2.94) takes now the form

Fig. 2.17 Energy level diagram for photons in a mode of the electromagnetic radiation field. Indicated is the effect of photon creation and annihilation operators, \hat{a}^+ and \hat{a} , respectively, onto the number states $|\mathcal{N}\rangle$



$$\hat{H}_F = \frac{\hbar\omega}{2}(\hat{a}^+\hat{a} + \hat{a}\hat{a}^+) = \hbar\omega\left(\hat{a}^+\hat{a} + \frac{1}{2}\right) \quad (2.100)$$

$$= \hbar\omega\left(\hat{\mathcal{N}} + \frac{1}{2}\right). \quad (2.101)$$

The derivation of the algebra for the operators $\hat{\mathcal{N}}$, \hat{a} and \hat{a}^+ is straight forward, based on the commutation rule (2.97). It can be found in all quantum mechanics text books. We thus only summarize here the results. The number operator $\hat{\mathcal{N}}$ is Hermitian (while \hat{a} and \hat{a}^+ are not). It has eigenstates $|\mathcal{N}\rangle$ with integer numbers \mathcal{N} as eigenvalues:

$$\hat{\mathcal{N}}|\mathcal{N}\rangle = \mathcal{N}|\mathcal{N}\rangle \quad (2.102)$$

$$\text{with } \mathcal{N} = 0, 1, 2, \dots \text{ and } \langle \mathcal{N} | \mathcal{N}' \rangle = \delta_{\mathcal{N}\mathcal{N}'}. \quad (2.103)$$

With this the eigenvalues of the Hamiltonian (2.101) follow immediately:

$$\hat{H}_F|\mathcal{N}\rangle = W_{\mathcal{N}}|\mathcal{N}\rangle \quad (2.104)$$

$$\text{where } W_{\mathcal{N}} = (\mathcal{N} + 1/2)\hbar\omega \text{ for } \mathcal{N} = 0, 1, 2, \dots \quad (2.105)$$

We recognize the well known eigenenergies of the harmonic oscillator. One interprets \mathcal{N} as the number of photons present in the particular resonator mode under consideration. Since photons are bosons, the mode may be populated with any number \mathcal{N} photons.

This is illustrated in the energy diagram Fig. 2.17. The levels of the harmonic oscillator are equally spaced, and the lowest energy is given by $\hbar\omega/2$, the “zero point energy”. Excitation of the \mathcal{N} th harmonic of the classical oscillator corresponds to a state occupied by \mathcal{N} photons.

The eigenstates $|\mathcal{N}\rangle$ of the number operator (and the harmonic oscillator) may be generated from the vacuum state $|0\rangle$ by repetitive application of the operator \hat{a}^+ for which

$$\hat{a}^+|\mathcal{N}\rangle = \sqrt{\mathcal{N}+1}|\mathcal{N}+1\rangle. \quad (2.106)$$

Hence, \hat{a}^+ is called *creation operator*. In contrast, the operator \hat{a} *reduces the photon number* by one, when applied to a number state

$$\hat{a}|\mathcal{N}\rangle = \sqrt{\mathcal{N}}|\mathcal{N}-1\rangle, \quad (2.107)$$

and hence \hat{a} is called *annihilation operator*. \mathcal{N} such operations lead to the *vacuum state* $|0\rangle$ for which the relation

$$\hat{a}|0\rangle \equiv 0 \quad (2.108)$$

must hold, since a nonexisting photon cannot be destructed any further. The inverse scheme starts with the vacuum state, from which one can generate any number state by $(\hat{a}^+)^{\mathcal{N}}|0\rangle = \sqrt{\mathcal{N}!}|\mathcal{N}\rangle$. The factors $\sqrt{\mathcal{N}+1}$ and $\sqrt{\mathcal{N}}$ in (2.106) and (2.107), respectively, make sure that the number states are correctly normalized as stated by (2.103).

Obviously, the number operator (2.99) counts the number of photons \mathcal{N} in the mode under consideration. This number is increased or decreased by one when the operator \hat{a}^+ and \hat{a} , respectively, acts on the photon states. Writing the Hamiltonian in the form (2.101) implies simply counting the occupation number. This procedure is called *second quantization* and may be applied to other quantum objects as well.

The evolution of the photon states with time $|\psi_{\mathcal{N}}(t)\rangle$ is obtained from the trivial time dependent SCHRÖDINGER equation

$$\hat{H}_F |\psi_{\mathcal{N}}(t)\rangle = i\hbar \frac{\delta}{\delta t} |\psi_{\mathcal{N}}(t)\rangle, \quad (2.109)$$

which is solved as usual by

$$|\psi_{\mathcal{N}}(t)\rangle = e^{-iW_{\mathcal{N}}t/\hbar} |\mathcal{N}\rangle = e^{-i(\mathcal{N}+\frac{1}{2})\omega_k t} |\mathcal{N}\rangle. \quad (2.110)$$

Note that in all this discussion the SCHRÖDINGER picture is used. All time dependence of the radiation field is now cast into the time dependence of the photon states. The operators \hat{a} and \hat{a}^+ are not time dependent.

2.3.2 The Electric Field Operator

Finally, we come back to the key question: how to quantize the electromagnetic field? Comparing the definition (2.96) for annihilation and creation operators with the classical field quantities (2.93) leads us immediately to operators for the electric

field (we resume now showing the indices $\mathbf{k}q$):¹¹

$$\widehat{E}_{\mathbf{k}q}^- = \sqrt{\frac{2\hbar\omega_{\mathbf{k}}}{L^3\varepsilon_0}} \hat{a}_{\mathbf{k}q} \quad \text{and} \quad \widehat{E}_{\mathbf{k}q}^+ = \sqrt{\frac{2\hbar\omega_{\mathbf{k}}}{L^3\varepsilon_0}} \hat{a}_{\mathbf{k}q}^+. \quad (2.111)$$

Again, in the SCHRÖDINGER picture these operators are independent of time. They have to be inserted into (2.87) in place of their classical counterparts. Thus, the electric field operator may be written as

$$\widehat{E}(\mathbf{r}, t) = \frac{i}{2} \sum_{\mathbf{k}q} \sqrt{\frac{2\hbar\omega_{\mathbf{k}}}{\varepsilon_0}} \{ \hat{a}_{\mathbf{k}} \mathbf{u}_{\mathbf{k}q}(\mathbf{r}) - \hat{a}_{\mathbf{k}}^+ \mathbf{u}_{\mathbf{k}q}^*(\mathbf{r}) \} \quad (2.112)$$

$$\text{with } \mathbf{u}_{\mathbf{k}q}(\mathbf{r}) = L^{-3/2} \mathbf{e}_q \exp(i\mathbf{k}\mathbf{r}). \quad (2.113)$$

Since creation and annihilation operators are defined dimensionless, one easily verifies that the unit of the electric field operator is indeed $[\widehat{E}] = \text{V m}^{-1}$. We point out that $\widehat{E}(\mathbf{r}, t)$ is a Hermitian operator (while its constituents $\hat{a}_{\mathbf{k}}$ and $\hat{a}_{\mathbf{k}}^+$ are not). We also mention here, that (2.112) is sufficiently flexible to adapt the quantization formalism for any specific experimental situation by an appropriate change of the modes (2.113) – e.g. for application to quantum optics in a cavity.

To obtain the *field energy* one has to insert (2.112) into (2.89) and evaluate it in full analogy to the classical considerations. However, now the commutation rule (2.97) must be observed. This finally leads to a sum of Hamiltonians (2.101) for all modes:

$$\widehat{H}_F = \frac{1}{2} \sum_{\mathbf{k}q} \hbar\omega_{\mathbf{k}} [\hat{a}_{\mathbf{k}q} \hat{a}_{\mathbf{k}q}^+ + \hat{a}_{\mathbf{k}q}^+ \hat{a}_{\mathbf{k}q}] = \sum_{\mathbf{k}q} \hbar\omega_{\mathbf{k}} \left[\hat{a}_{\mathbf{k}q}^+ \hat{a}_{\mathbf{k}q} + \frac{1}{2} \right]. \quad (2.114)$$

2.3.3 GLAUBER States

It is important to realize that the photon number states introduced above do not represent coherent light. Rather, coherent light must be described by a linear superposition of many number states as shown for the first time by GLAUBER (1963). For a single mode, these so called *GLAUBER states (also coherent photon states)* are given by

$$|\alpha\rangle = \exp\left(-\frac{1}{2}|\alpha|^2\right) \sum_{\mathcal{N}} \frac{\alpha^{\mathcal{N}}}{(\mathcal{N}!)^{1/2}} |\mathcal{N}\rangle \quad (2.115)$$

¹¹We mention that GLAUBER (1963) uses time dependent field operators (HEISENBERG picture) and a slightly different notation. He writes (in [esu](#)) “the positive frequency part of the electric field operator”

$$\mathbf{E}^{(+)}(\mathbf{r}, t) = i \sum_{\mathbf{k}} \sqrt{\hbar\omega/2} a_{\mathbf{k}} \mathbf{u}_{\mathbf{k}}(\mathbf{r}) e^{-i\omega_{\mathbf{k}}t}.$$

$$\text{and } \langle \alpha | = \exp\left(-\frac{1}{2}|\alpha|^2\right) \sum_{\mathcal{N}} \frac{\alpha^{*\mathcal{N}}}{(\mathcal{N}!)^{1/2}} \langle \mathcal{N} |.$$

Let us have a brief look at the properties of GLAUBER states.

We first note that they are normalized,

$$\langle \alpha | \alpha \rangle = \exp(-|\alpha|^2) \sum_{\mathcal{N}} \frac{\alpha^{*\mathcal{N}} \alpha^{\mathcal{N}}}{\mathcal{N}!} = 1, \quad (2.116)$$

as the sum corresponds to the exponential function $\exp(|\alpha|^2)$. They are, however, not orthonormal, rather we have

$$\langle \alpha | \beta \rangle = \exp\left(-\frac{1}{2}|\alpha|^2 - \frac{1}{2}|\beta|^2\right) \sum_{\mathcal{N}} \frac{\alpha^{*\mathcal{N}} \beta^{\mathcal{N}}}{\mathcal{N}!} \exp\left(-\frac{1}{2}|\alpha|^2 - \frac{1}{2}|\beta|^2 - \alpha^* \beta\right),$$

and for the absolute squared of this scalar product one obtains

$$|\langle \alpha | \beta \rangle|^2 = \exp(-|\alpha - \beta|^2). \quad (2.117)$$

This set of coherent states is thus overcomplete, i.e. there are more coherent states than number states $|\mathcal{N}\rangle$. From (2.117) we see, however, that two GLAUBER states get *nearly* orthogonal, if $|\alpha - \beta| \gg 1$. Applying the photon annihilation operator onto (2.115), we obtain with (2.107)

$$\begin{aligned} \hat{a}|\alpha\rangle &= \exp\left(-\frac{1}{2}|\alpha|^2\right) \sum_{\mathcal{N}} \frac{\alpha^{\mathcal{N}}}{(\mathcal{N}!)^{1/2}} \mathcal{N}^{1/2} |\mathcal{N}-1\rangle \\ &= \alpha \exp\left(-\frac{1}{2}|\alpha|^2\right) \sum_{\mathcal{N}} \frac{\alpha^{\mathcal{N}-1}}{((\mathcal{N}-1)!)^{1/2}} |\mathcal{N}-1\rangle = \alpha|\alpha\rangle. \end{aligned} \quad (2.118)$$

GLAUBER states are thus eigenstates of the photon annihilation operator \hat{a} . One may extract photons of a GLAUBER state without changing that state. *Conversely*, $|\alpha\rangle$ is not an eigenstate of the photon creation operator. It is important to note, that with (2.111) single mode GLAUBER states are also eigenstates of the field operator \hat{E}^- (but not of its conjugate counter part). Measuring electromagnetic fields usually implies that photons are registered, i.e. a photon is extracted from the radiation field. If the field can be described by a GLAUBER state $|\alpha\rangle$, the detectable probability amplitude will thus be proportional to $\langle \alpha | \hat{E}^- | \alpha \rangle \propto \alpha$. This is in essence what makes GLAUBER states coherent. Since the characteristic parameter α can also be complex, α may be seen to represent phase *and* amplitude of the electromagnetic field.

The expectation values of the annihilation and creation operators in a GLAUBER state follow from (2.118) and by applying (2.106) onto (2.115), respectively:

$$\langle \alpha | \hat{a} | \alpha \rangle = \alpha \quad \text{and} \quad \langle \alpha | \hat{a}^+ | \alpha \rangle = \alpha^*. \quad (2.119)$$

Finally we have to obtain a relation between a GLAUBER state and the intensity of the radiation. Let us first note that the population of photon number states $|\mathcal{N}\rangle$ in a GLAUBER state is given by a POISSON distribution

$$p_{\mathcal{N}} = |\langle \mathcal{N} | \alpha \rangle|^2 = \exp(-|\alpha|^2) \frac{|\alpha|^{2\mathcal{N}}}{\mathcal{N}!}. \quad (2.120)$$

The expectation value of the photon number operator (2.99) in a state $|\alpha\rangle$, i.e. the mean photon number $\overline{\mathcal{N}}$ in a GLAUBER state, is

$$\overline{\mathcal{N}} = \langle \alpha | \hat{\mathcal{N}} | \alpha \rangle = \exp(-|\alpha|^2) \sum_{\mathcal{N}} \frac{\alpha^{*\mathcal{N}} \alpha^{\mathcal{N}}}{\mathcal{N}!} \mathcal{N} = |\alpha|^2. \quad (2.121)$$

In this context we recall a well known property of the POISSON distribution: its standard deviation is given by

$$\Delta \mathcal{N} = \frac{\sqrt{\langle \alpha | \hat{\mathcal{N}}^2 | \alpha \rangle - \langle \alpha | \hat{\mathcal{N}} | \alpha \rangle^2}}{\langle \alpha | \hat{\mathcal{N}} | \alpha \rangle} = |\alpha| = \sqrt{\overline{\mathcal{N}}}. \quad (2.122)$$

This is actually *very good news for all of our following discussion*. A look at Table 2.2 shows that for lasers – the light source typically used today in spectroscopy – the number of photons per mode is extremely large. And since $\sqrt{\overline{\mathcal{N}}}/\overline{\mathcal{N}} = 1/\sqrt{\overline{\mathcal{N}}}$, the *relative width of the distribution of photon numbers is very small* (e.g. for the dye laser mentioned in Table 2.2 on the order of 10^{-6}). Thus, for all intents and purposes in spectroscopy, *we may represent the ideal, coherent GLAUBER state by a pure number state $|\mathcal{N}\rangle$* , where \mathcal{N} represents the *average number of photons $\overline{\mathcal{N}}$ per mode* according to (2.84). With this – extremely good – approximation the derivation and application of optical transition probabilities given below can be accomplished without any mathematical difficulties.

Although the GLAUBER states considered here refer to a single occupied mode only, they provide a good description for a sufficiently intense, quasi-monochromatic and well collimated radiation field, such as a laser beam (one may even adapt the modes (2.113) suitably).

Quantitatively, we derive the expectation value of the electric field operator (2.112) with the help of (2.119)

$$\langle \alpha | \hat{\mathbf{E}} | \alpha \rangle = i C_k (\alpha \mathbf{e} \cdot \mathbf{e}^{i\mathbf{k}\mathbf{r}} - \alpha^* \mathbf{e}^* \cdot \mathbf{e}^{-i\mathbf{k}\mathbf{r}}) \quad \text{with } C_k = \sqrt{\frac{\hbar \omega_k}{2L^3 \epsilon_0}}. \quad (2.123)$$

At very high (classical) intensities when representing a GLAUBER states by a single photon number state with $\mathcal{N} = \overline{\mathcal{N}}$, with (2.121) we can set with sufficient accuracy

$$|\alpha| = \sqrt{\overline{\mathcal{N}}} \simeq \sqrt{\mathcal{N}} \simeq \sqrt{\mathcal{N} + 1}. \quad (2.124)$$

Comparing this to the spatial part of the classical field according to (1.35)

$$\mathbf{E}(\mathbf{r}) = \frac{i}{2} E_0 (\mathbf{e} e^{i\mathbf{k}\mathbf{r}} - \mathbf{e}^* e^{-i\mathbf{k}\mathbf{r}}) \quad (2.125)$$

we can relate the amplitude $E_0 = 2C_k\alpha$ of the classical, single mode field to the number of photons in the mode:

$$\sqrt{\mathcal{N}} \simeq \sqrt{\mathcal{N}+1} \simeq |\alpha| = \frac{|E_0|}{2C_k} = \sqrt{\frac{I_0}{c\hbar\omega}} L^3. \quad (2.126)$$

In the last step we have used the standard relation $I_0 = \varepsilon_0 c |E_0|^2 / 2$ between intensity and field amplitude. We mention that this relation is equivalent to (2.86), with \mathcal{N} being the number of photons in the (presently thus defined) coherence volume L^3 . In the general case of radiation with a finite bandwidth and divergence angle, \mathcal{N} has to be identified with (2.84).

2.3.4 Addendum for Multi-Mode States

As discussed above the average number of photon per mode in a typical laser beam may be very high and a classical, coherent radiation field will be described by GLAUBER states. However, in principle the photon number states $|0\rangle, |1\rangle, \dots, |\mathcal{N}\rangle \dots$ can be found also with quite different populations – and thus represent different coherence properties of the radiation field. This is a key theme of *modern quantum optics*.

Here we just add a few remarks relevant to multi-mode states as needed to describe any realistic radiation field in some detail. These states are typically written as products of single particle states.¹² As the most simple case we discuss here only products of pure number states which by the arguments given in the preceding subsection can be a valid description of a quasi-monochromatic laser beam:

$$|\{\mathcal{N}_{kq}\}\rangle = |\mathcal{N}_1\rangle |\mathcal{N}_2\rangle \dots |\mathcal{N}_i\rangle |\dots\rangle = |\mathcal{N}_1 \mathcal{N}_2 \dots \mathcal{N}_i \dots\rangle. \quad (2.127)$$

Such a state describes an electromagnetic field with $\mathcal{N}_1, \mathcal{N}_2, \dots, \mathcal{N}_i, \dots$ photons in modes characterized by $\mathbf{k}_1, \mathbf{k}_2, \dots, \mathbf{k}_i, \dots$ and polarization vectors $\mathbf{e}_1, \mathbf{e}_2, \dots, \mathbf{e}_i, \dots$. The respective creation and annihilation operators generate or annihilate one photon in a specific mode according to the scheme

$$\begin{aligned} \hat{a}_{\mathbf{k}_i q_i}^+ |\{\mathcal{N}_{kq}\}\rangle &= \hat{a}_{\mathbf{k}_i q_i}^+ |\mathcal{N}_1 \dots \mathcal{N}_i \dots\rangle = \sqrt{\mathcal{N}_i + 1} |\mathcal{N}_1 \dots \mathcal{N}_i + 1 \dots\rangle \\ \hat{a}_{\mathbf{k}_i q_i} |\{\mathcal{N}_{kq}\}\rangle &= \hat{a}_{\mathbf{k}_i q_i} |\mathcal{N}_1 \dots \mathcal{N}_i \dots\rangle = \sqrt{\mathcal{N}_i} |\mathcal{N}_1 \dots \mathcal{N}_i - 1 \dots\rangle \\ \hat{a}_{\mathbf{k}_i q_i} |\mathcal{N}_1 \dots 0 \dots\rangle &\equiv 0. \end{aligned} \quad (2.128)$$

Since each of these operators acts only onto one of the modes, the commutation rule (2.97) is now generalized by

$$[\hat{a}_{kq}, \hat{a}_{k'q'}^+] = \delta_{kk'} \delta_{qq'} \quad \text{while} \quad [\hat{a}_{kq}, \hat{a}_{k'q'}] = [\hat{a}_{kq}^+, \hat{a}_{k'q'}^+] \equiv 0. \quad (2.129)$$

¹²A different situation is encountered with so called entangled states – an interesting subject but beyond our present scope. See also Appendix E.3 in Vol. 1.

The multi-mode number states are orthonormalized:

$$\langle \mathcal{N}_1 \mathcal{N}_2 \dots \mathcal{N}_i \dots | \mathcal{N}'_1 \mathcal{N}'_2 \dots \mathcal{N}'_i \dots \rangle = \delta_{\mathcal{N}_1 \mathcal{N}'_1} \delta_{\mathcal{N}_2 \mathcal{N}'_2} \dots \delta_{\mathcal{N}_i \mathcal{N}'_i} \dots \quad (2.130)$$

Their total Hamiltonian is given by (2.114).

We now have all necessary tools to describe a more or less quasi-monochromatic light beam with small or even larger divergence in quantum mechanical terms. We must, however, keep in mind – as described in detail in Sects. 2.1.1–2.1.7 – that an arbitrary classical radiation field is not a simple linear superposition of plane waves. Neither can we describe the quantized radiation field by a linear superposition of $|\{\mathcal{N}_{\mathbf{k}q}\}\rangle$ states – except in the special case of a fully coherent state. As in the classical case (Sect. 2.1.4), the field is defined by a distribution $\langle E^-(\mathbf{k}) E^+(\mathbf{k}') \rangle$ of amplitudes and frequencies (or wave vectors). In the classical case this distribution was found to be diagonal in \mathbf{k} . This also holds for the quantum description.

It will be sufficient to specify the probability amplitudes for the states

$$|\mathcal{N}_1 00 \dots 0\rangle, |0 \mathcal{N}_2 0 \dots 0\rangle, |00 \mathcal{N}_3 \dots 0\rangle, \dots, |00 \dots \mathcal{N}_i \dots 0\rangle, \dots \quad (2.131)$$

in a range of relevant modes $\mathbf{k}_i q_i$ where \mathcal{N}_i refers to the average number of photons in that particular mode. The proper quantum mechanical tool for the necessary book keeping is the density matrix. Chapter 9 will give an introduction into the density matrix formalism. Quantitative treatments can become rather involved (see e.g. MUKAMEL 1999).

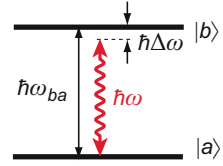
2.3.5 Interaction Hamiltonian for Dipole Transitions

As in the semiclassical treatment the interaction energy is dominated by the dipole energy. As an excellent approximation one neglects again the wavelength dependence of the electric field on the position \mathbf{r} within the atom, since at least for the IR, VIS and UV spectral range the wavelength is large compared to atomic dimensions, $\mathbf{k} \cdot \mathbf{r} \ll 1$. Thus, $\exp(i\mathbf{k} \cdot \mathbf{r}) \simeq 1$ and we shall limit the discussion here exclusively to electric dipole (E1) transitions (a generalization, if needed, can be obtained following the corresponding considerations in Sect. 5.4, Vol. 1).

As already emphasized, we use the SCHRÖDINGER picture with a time independent perturbation,¹³ and translate the semiclassical treatment of radiation induced transitions (Chap. 4 in Vol. 1) into the fully quantized description. With the field operator (2.112) the interaction Hamiltonian between atom and field is given in

¹³One could also use the HEISENBERG picture with a time dependent field operator and time independent states. The final result would be the same.

Fig. 2.18 Schematic of a level system



analogy to (4.55), Vol. 1 by¹⁴

$$\begin{aligned}\hat{U}(\mathbf{r}) &= e\mathbf{r} \cdot \hat{\mathbf{E}} = -\mathcal{D} \cdot \hat{\mathbf{E}} = i \sum_{\mathbf{k}} \sqrt{\frac{\hbar\omega_{\mathbf{k}}}{2L^3\epsilon_0}} e\mathbf{r} \cdot [\mathbf{e}\hat{a}_{\mathbf{k}} - \mathbf{e}^*\hat{a}_{\mathbf{k}}^+] \\ &= i \sum_{\mathbf{k}} eC_{\mathbf{k}} [\hat{\mathbf{D}}\hat{a}_{\mathbf{k}} - \hat{\mathbf{D}}^\dagger\hat{a}_{\mathbf{k}}^+], \quad \text{with } C_{\mathbf{k}} = \sqrt{\frac{\hbar\omega_{\mathbf{k}}}{2L^3\epsilon_0}}\end{aligned}\quad (2.132)$$

and the dipole transition operators $\hat{\mathbf{D}} = \mathbf{r} \cdot \mathbf{e}$ and $\hat{\mathbf{D}}^\dagger = \mathbf{r} \cdot \mathbf{e}^*$,

for absorption and emission of a photon with polarization \mathbf{e} , respectively. For convenience of writing we have here again pulled the elementary charge e out from the electron dipole moment $\mathcal{D} = -e\mathbf{r}$.¹⁵

As expected, in contrast to (4.55), Vol. 1 the interaction Hamiltonian (2.132) is now time independent and documents energy conservation: in this fully quantized picture *energy is simply exchanged* between atomic and photonic states.

Before we derive the matrix elements of the interaction Hamiltonian \hat{U} , we point out that each relevant mode \mathbf{k}, \mathbf{e} in the sum (2.132) contains two parts: the first part (with $\hat{a}_{\mathbf{k}}$) destroys a photon (in a mode with the wave vector \mathbf{k} and the polarization vector \mathbf{e}) and corresponds to absorption, while the second part (with $\hat{a}_{\mathbf{k}}^+$) generates a photon (in a corresponding mode) and describes emission. We recall that in the semiclassical description of the electromagnetic field (2.87) these two terms correspond to the positive and negative frequency part, respectively.

Without interaction between field and atomic system *the eigenstates of the total system may be written as product states* $|\psi; \{\mathcal{N}_i\}\rangle$ of atomic states $|\psi\rangle$ and photon states $|\mathcal{N}\rangle$ according to (2.127).

If the spectral intensity distribution of the radiation is close to a resonance of the atomic system – as sketched in Fig. 2.18 – a *two level system* is a usually a good approximation. The eigenfunction of $|\psi\rangle$ then corresponds to either upper or

¹⁴As in the semiclassical description we apply the dipole length approximation. In dipole velocity approximation the quantized perturbation reads

$$\hat{U}_v(\mathbf{r}) = i \sum_{\mathbf{k}\mathbf{e}} \sqrt{\frac{\hbar}{2L^3\epsilon_0\omega_{\mathbf{k}}}} \frac{e}{m_e} \hat{\mathbf{p}} \cdot [\mathbf{e}\hat{a}_{\mathbf{k}} + \mathbf{e}^*\hat{a}_{\mathbf{k}}^+].$$

With exact eigenfunctions both approximations lead to the same transition probabilities.

¹⁵If more than one active electrons are involved, one has to replace the position vector \mathbf{r} by a sum over all \mathbf{r}_i for the active electrons.

lower state, $|b\rangle$ and $|a\rangle$, respectively, while $\mathcal{N}_1, \mathcal{N}_2 \dots \mathcal{N}_i \dots$ defines the number of photons in the modes $\mathbf{k}_1, \mathbf{k}_2 \dots \mathbf{k}_i \dots$. The matrix elements of the interaction Hamiltonian (2.132) are given by:

$$\begin{aligned} \langle b; \{\mathcal{N}'_i\} | \widehat{U} | a; \{\mathcal{N}_i\} \rangle &= \langle b; \mathcal{N}'_1 \mathcal{N}'_2 \dots \mathcal{N}'_i \dots | e \mathbf{r} \cdot \widehat{\mathbf{E}} | a; \mathcal{N}_1 \mathcal{N}_2 \dots \mathcal{N}_i \dots \rangle \\ &= i \sum_{\mathbf{k}} e C_k [\widehat{\mathbf{D}}_{ba} \langle \mathcal{N}'_1 \dots \mathcal{N}'_i \dots | \hat{a}_{\mathbf{k}} | \mathcal{N}_1 \dots \mathcal{N}_i \dots \rangle \\ &\quad - \widehat{\mathbf{D}}_{ba}^{\dagger} \langle \mathcal{N}'_1 \dots \mathcal{N}'_i \dots | \hat{a}_{\mathbf{k}}^{\dagger} | \mathcal{N}_1 \dots \mathcal{N}_i \dots \rangle]. \end{aligned} \quad (2.133)$$

The latter rearrangement is possible since \mathbf{r} acts only onto the atomic part, while $\hat{a}_{\mathbf{k}}$ and $\hat{a}_{\mathbf{k}}^{\dagger}$ (and thus $\widehat{\mathbf{E}}$) act only onto the photon part of the system. The *matrix elements of the dipole transition operators for absorption and emission* are the same as (4.57), Vol. 1, elaborated for the semiclassical treatment in Sect. 4.3.4, Vol. 1:

$$\widehat{\mathbf{D}}_{ba} = \mathbf{r}_{ba} \cdot \mathbf{e} \quad \text{and} \quad \widehat{\mathbf{D}}_{ab}^{\dagger} = \mathbf{r}_{ab} \cdot \mathbf{e}^* = \mathbf{r}_{ba}^* \cdot \mathbf{e}^* = \widehat{\mathbf{D}}_{ba}^* \quad (2.134)$$

$$\text{with } \mathbf{r}_{ba} = \langle b | \mathbf{r} | a \rangle = \int \psi_b^*(\mathbf{r}) \mathbf{r} \psi_a(\mathbf{r}) d^3 \mathbf{r} = \mathbf{r}_{ab}^*.$$

Since \mathbf{r} has odd parity, $|b\rangle$ and $|a\rangle$ must have different parity. According to (2.128), the operators $\hat{a}_{\mathbf{k}}^{\dagger}$ and $\hat{a}_{\mathbf{k}}$ create or annihilate a photon of one specific mode and polarization. And the photon states are orthogonal according to (2.130). The matrix element of the \widehat{U} is thus zero unless $\mathcal{N}'_i = \mathcal{N}_i \pm 1$ holds for one of the photon states, while all others are the same before and after the transition. For one single occupied mode, i.e. for $\mathcal{N}_{\mathbf{k}\mathbf{e}}$ photons with momentum $\hbar \mathbf{k}$ and polarization \mathbf{e} , the nonvanishing matrix elements (2.133) may be written in compact form:

$$\begin{aligned} \langle b \mathcal{N}_{\mathbf{k}\mathbf{e}} - 1 | \widehat{U} | a \mathcal{N}_{\mathbf{k}\mathbf{e}} \rangle &= \langle b | \widehat{\mathbf{D}} | a \rangle \langle \mathcal{N}_{\mathbf{k}\mathbf{e}} - 1 | i \hat{a}_{\mathbf{k}} | \mathcal{N}_{\mathbf{k}\mathbf{e}} \rangle \\ &= i \widehat{\mathbf{D}}_{ba} e C_k \sqrt{\mathcal{N}_{\mathbf{k}\mathbf{e}}} \end{aligned} \quad (2.135a)$$

$$\begin{aligned} \langle a \mathcal{N}_{\mathbf{k}\mathbf{e}} - 1 | \widehat{U} | b \mathcal{N}_{\mathbf{k}\mathbf{e}} \rangle &= \langle a | \widehat{\mathbf{D}} | b \rangle \langle \mathcal{N}_{\mathbf{k}\mathbf{e}} - 1 | i \hat{a}_{\mathbf{k}} | \mathcal{N}_{\mathbf{k}\mathbf{e}} \rangle \\ &= i \widehat{\mathbf{D}}_{ab} e C_k \sqrt{\mathcal{N}_{\mathbf{k}\mathbf{e}}} \end{aligned} \quad (2.135b)$$

$$\begin{aligned} \langle a \mathcal{N}_{\mathbf{k}\mathbf{e}} + 1 | \widehat{U} | b \mathcal{N}_{\mathbf{k}\mathbf{e}} \rangle &= \langle a | \widehat{\mathbf{D}}^{\dagger} | b \rangle \langle \mathcal{N}_{\mathbf{k}\mathbf{e}} + 1 | -i \hat{a}_{\mathbf{k}}^{\dagger} | \mathcal{N}_{\mathbf{k}\mathbf{e}} \rangle \\ &= -i \widehat{\mathbf{D}}_{ab}^{\dagger} e C_k \sqrt{\mathcal{N}_{\mathbf{k}\mathbf{e}} + 1} \end{aligned} \quad (2.135c)$$

$$\begin{aligned} \langle b \mathcal{N}_{\mathbf{k}\mathbf{e}} + 1 | \widehat{U} | a \mathcal{N}_{\mathbf{k}\mathbf{e}} \rangle &= \langle b | \widehat{\mathbf{D}}^{\dagger} | a \rangle \langle \mathcal{N}_{\mathbf{k}\mathbf{e}} + 1 | -i \hat{a}_{\mathbf{k}}^{\dagger} | \mathcal{N}_{\mathbf{k}\mathbf{e}} \rangle \\ &= -i \widehat{\mathbf{D}}_{ba}^{\dagger} e C_k \sqrt{\mathcal{N}_{\mathbf{k}\mathbf{e}} + 1}. \end{aligned} \quad (2.135d)$$

Here C_k is the field normalization constant used in (2.132), originating from proper calibration of the total field energy (2.114). When deriving (2.135a)–(2.135d) from (2.133) we have used (2.106) and (2.107). The somewhat abstract number $\mathcal{N}_{\mathbf{k}\mathbf{e}}$ of photons per mode can be related by (2.84) to the (measurable) spectral intensity distribution $\tilde{I}(\omega_{\mathbf{k}})$.

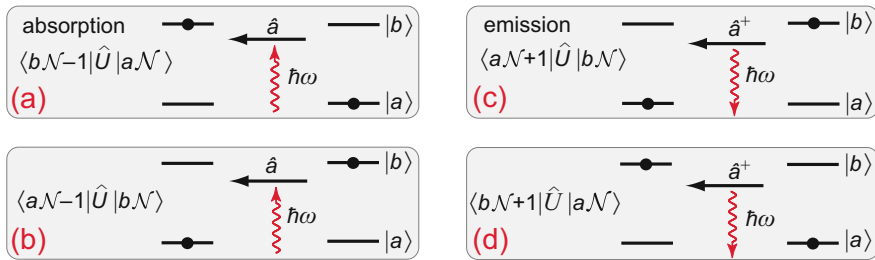


Fig. 2.19 Interaction matrix elements between atom and field, schematically; (a)–(d) refer to equations (2.135a)–(2.135d), respectively

The physical interpretation of the matrix elements is schematically explained in Fig. 2.19. As summarized for the semiclassical treatment in (4.53), Vol. 1, only two of these matrix elements are relevant within the framework of 1st order perturbation theory:

- Figure 2.19(a) symbolizes absorption (annihilation) of a photon, accompanied by excitation of the system from a lower state $|a\rangle$ into an upper state $|b\rangle$ according to (2.135a),
- Figure 2.19(c) symbolizes emission (creation) of a photon, accompanied by de-excitation of the system from an upper state $|b\rangle$ into a lower state $|a\rangle$ according to (2.135c).

The other two nonvanishing matrix elements correspond to so called “virtual de-excitation” (Fig. 2.19(b)) and “virtual excitation” (Fig. 2.19(d)) processes by absorption and emission of a photon, respectively. These processes are not energy conserving and do not play a role in 1st order perturbation theory, as we shall see in a moment. However, they are of crucial importance in the description of higher order processes, such as multi-photon excitation or ionization in strong fields, as well as for RAMAN scattering and other nonlinear processes.

We finally note that – if necessary – \hat{D}_{ba} may be modified appropriately as in the semiclassical description to describe other types of transitions, such as E2 and M1.

2.3.6 Perturbation Theory and Spontaneous Emission

We shall use again 1st order perturbation theory to describe E1 transitions. Even though this approach has its limitations, to be discussed at the end of this section, we shall be able now to derive a rate for spontaneous emission, which was not possible with the semiclassical approach. In any case, the following, fully quantized treatment of radiation induced transitions will form the basis for later, more rigorous treatments, e.g. in Chap. 10.

We consider an effective two level system with the atomic states $|a\rangle$ and $|b\rangle$ being nearly in resonance with the radiation as indicated in Fig. 2.18. Let \hat{H}_A be

the Hamiltonian for the free atom, \hat{H}_F that of the free field (2.114). The stationary SCHRÖDINGER equation for the unperturbed atom is

$$\hat{H}_A|b\rangle = \hbar\omega_b|b\rangle \quad \text{and} \quad \hat{H}_A|a\rangle = \hbar\omega_a|a\rangle, \quad (2.136)$$

with a transition frequency $\omega_{ba} = \omega_b - \omega_a > 0$, while

$$\hat{H}_F|\mathcal{N}_{\mathbf{k}\mathbf{e}}\rangle = \mathcal{N}_{\mathbf{k}\mathbf{e}}\hbar\omega_{\mathbf{k}}|\mathcal{N}_{\mathbf{k}\mathbf{e}}\rangle \quad (2.137)$$

describes a state of $\mathcal{N}_{\mathbf{k}\mathbf{e}}$ photons in a mode \mathbf{k} with polarization \mathbf{e} . We start our derivation again with a single occupied field mode and sum later on over all field modes. That is possible without problems due to the orthogonality relation (2.130). The corresponding time dependent SCHRÖDINGER equation

$$i\hbar \frac{\partial |\psi(t)\rangle}{\partial t} = (\hat{H}_0 + \hat{U})|\psi(t)\rangle = (\hat{H}_A + \hat{H}_F + \hat{U})|\psi(t)\rangle \quad (2.138)$$

has to be solved with the interaction \hat{U} according to (2.132).

Note that *the full Hamiltonian $\hat{H}_A + \hat{H}_F + \hat{U}$ for atom, field and interaction is still time independent.* Hence, energy conservation holds in this fully quantized SCHRÖDINGER picture – in contrast to the semiclassical radiation theory (4.40), Vol. 1, where the interaction was time dependent. Thus, we have to find stationary solutions of (2.138). We shall do this indeed in Chap. 10. For the moment we are simply interested in *all possible transitions which are induced by switching the interaction on.* Quite generally, one may expand $|\psi(t)\rangle$ into a series of unperturbed eigenfunctions of the system:

$$|\psi(t)\rangle = \sum_{\mathcal{N}j} c_{j\mathcal{N}}(t) |j\mathcal{N}\rangle e^{-i(\omega_j + \mathcal{N}\omega)t}. \quad (2.139)$$

Here $c_{j\mathcal{N}}$ is the probability amplitude for finding \mathcal{N} photons in the field while the atom is found in state $|j\rangle$. For simplicity of writing we have dropped again the indices \mathbf{k} and \mathbf{e} for the photon states \mathcal{N} and for the angular frequency ω of the field. We insert (2.139) into (2.138), multiply from the left with $\langle b\mathcal{N}'|$ or $\langle a\mathcal{N}'|$, and obtain two sets of differential equations for $c_{b\mathcal{N}}$ and $c_{a\mathcal{N}}$, respectively:

$$\begin{aligned} \frac{dc_{b\mathcal{N}}(t)}{dt} &= -\frac{i}{\hbar} \sum_{\mathcal{N}'} c_{a\mathcal{N}'} \langle b\mathcal{N}' | \hat{U} | a\mathcal{N} \rangle e^{i[(\mathcal{N}' - \mathcal{N})\omega + \omega_{ba}]t} \\ \frac{dc_{a\mathcal{N}}(t)}{dt} &= -\frac{i}{\hbar} \sum_{\mathcal{N}'} c_{b\mathcal{N}'} \langle a\mathcal{N}' | \hat{U} | b\mathcal{N} \rangle e^{i[(\mathcal{N}' - \mathcal{N})\omega - \omega_{ba}]t}. \end{aligned} \quad (2.140)$$

We have exploited the fact that *only matrix elements between different atomic states are non-zero.* We insert now the matrix elements (2.135a)–(2.135d). Since only the terms with $\mathcal{N}' = \mathcal{N} \pm 1$ are non-zero, two types of exponential factors appear in (2.140):

- energy conserving terms $\exp[\pm i(\omega - \omega_{ba})t]$ and
- non-energy conserving terms with $\exp[\pm i(\omega + \omega_{ba})t]$.

As we have seen already in Sect. 4.3.2, Vol. 1, in a perturbation treatment these terms are weighted with resonance denominators of the type $1/(\omega - \omega_{ba})$ and $1/(\omega + \omega_{ba})$. We now focus on the nearly resonant situation

$$|\Delta\omega| = |\omega - \omega_{ba}| \ll \omega_{ba}, \quad (2.141)$$

but allow nevertheless for small detuning $\Delta\omega$, as indicated in Fig. 2.18. In typical spectroscopic applications we shall have to account for detuning on the order of 10^8 s^{-1} , which are to be compared with transition frequencies on the order of 10^{15} s^{-1} . Thus, to a very good approximation the non-resonant terms $1/(\omega + \omega_{ba})$ can be neglected. This approximation is called *rotating wave approximation (RWA)*, since the terms $\exp[\pm i(\omega - \omega_{ba})t]$ imply, so to say, that the system follows the field in phase, while the others rotate in the opposite sense and thus average out with time.¹⁶

Consequently, this simplifies (2.140) substantially. Inserting (2.135a)–(2.135d) for the matrix elements this leads for the two level system to a simple set of two coupled equations

$$\dot{c}_{b\mathcal{N}} = \frac{eC_k}{\hbar} \sqrt{\mathcal{N}+1} \hat{\mathbf{D}}_{ba} c_{a\mathcal{N}+1} e^{i(\omega_{ba}-\omega)t} \quad (2.142)$$

$$\dot{c}_{a\mathcal{N}+1} = -\frac{eC_k}{\hbar} \sqrt{\mathcal{N}+1} \hat{\mathbf{D}}_{ba}^* c_{b\mathcal{N}} e^{-i(\omega_{ba}-\omega)t}, \quad (2.143)$$

with $C_k \propto \sqrt{\omega}$ being the field normalizing constant in (2.132). To derive the absorption probability we now assume, as in the semiclassical case, that at time $t = 0$ all atoms are in the lower state $|a\rangle$. We also assume that the photons in the mode \mathbf{k} with polarization \mathbf{e} are represented sufficiently well by a photon number state $|\mathcal{N}\rangle$. Thus, our initial conditions are

$$c_{a\mathcal{N}}(0) = 1 \quad \text{and} \quad c_{j\mathcal{N}'}(0) \equiv 0 \quad \text{for all } j, \mathcal{N}' \neq a, \mathcal{N}. \quad (2.144)$$

In 1st order perturbation theory one assumes in addition that $c_{a\mathcal{N}} \simeq 1$ remains constant. Thus, (2.142) may be integrated directly to obtain the probability amplitude $c_{b\mathcal{N}-1}(t)$ for finding $|b, \mathcal{N}-1\rangle$, i.e. for a transition of the system into the excited state $|b\rangle$ by annihilation of a photon. During this process one of the originally \mathcal{N} photons in mode \mathbf{k} is absorbed, so that in complete analogy to the classical case (4.58), Vol. 1 we have

$$c_{b\mathcal{N}-1}(t) = \frac{eC_k \sqrt{\mathcal{N}}}{\hbar} \hat{\mathbf{D}}_{ba} \frac{e^{i(\omega_{ba}-\omega)t} - 1}{i(\omega_{ba} - \omega)}. \quad (2.145)$$

¹⁶Originally this terminology was coined by microwave and radio frequency spectroscopy (EPR and NMR), where this phase reflects indeed a real physical rotation of the spin, induced by the exciting field.

The transition probability per unit of time is again $|c_{b\mathcal{N}-1}(t)|^2/t$. This leads to a transition rate

$$dR_{ba}^{(\mathcal{N}_k)} = \frac{2\pi}{\hbar^2} e^2 C_k^2 |\widehat{D}_{ba}|^2 \mathcal{N}_{ke} g(\omega_k) = \frac{\pi \omega_k e^2}{L^3 \varepsilon_0 \hbar} |\widehat{D}_{ba}|^2 \mathcal{N}_{ke} g(\omega_k) \quad (2.146)$$

induced by the \mathcal{N}_{ke} photons in the mode. We have now reintroduced the indices for polarization \mathbf{e} and wave vector \mathbf{k} of the radiation. With $g(\omega_k)$ we identify again the line profile as introduced in Sect. 4.3.5, Vol. 1. Integrated over all frequencies it is normalized to unity.

Completely equivalent one assumes for the de-excitation process $|b\rangle \rightarrow |a\rangle$ initial conditions

$$c_{b\mathcal{N}}(0) = 1 \quad \text{and} \quad c_{j\mathcal{N}'}(0) \equiv 0 \quad \text{for all } j, \mathcal{N}' \neq a, \mathcal{N}. \quad (2.147)$$

By integration of (2.143) one derives the probability amplitude for finding the system in a state $|a\mathcal{N}+1\rangle$. From this the transition rate for $a \leftarrow b$ by emission of a photon into the mode \mathbf{k}, \mathbf{e} is obtained:

$$dR_{ab}^{(\mathcal{N}_k)} = \frac{\pi \omega_k e^2}{L^3 \varepsilon_0 \hbar} |\widehat{D}_{ab}|^2 (\mathcal{N}_{ke} + 1) g(\omega_k). \quad (2.148)$$

So far the derivation was completely analogous to the semiclassical approximation. Now we have to recall, however, that there are $dm_{\omega\mathbf{e}}$ modes per frequency interval $d\omega_k$ and solid angle element $d\Omega$, with $dm_{\omega\mathbf{e}}$ given by (2.73). We thus find the absorption or emission probability into *given solid angle* $d\Omega$ element by integration over all available angular frequencies of the electromagnetic radiation inducing the transition. This leads to a rate

$$\begin{aligned} dR_{ba} &= \int dR_{ba}^{(\mathcal{N}_k)} dm_{\omega\mathbf{e}} = \frac{\pi e^2 L^3}{L^3 \varepsilon_0 \hbar^2} d\Omega \int_{-\infty}^{+\infty} d\omega_k \frac{\omega^2}{(2\pi c)^3} |\widehat{D}_{ba}|^2 \mathcal{N}_{ke} \hbar \omega_k g(\omega_k) \\ &= d\Omega \frac{\pi e^2}{\varepsilon_0 \hbar^2} \frac{\omega_{ba}^2}{(2\pi c)^3} |\widehat{D}_{ba}|^2 \mathcal{N}_{ke} \hbar \omega_{ba}. \end{aligned} \quad (2.149)$$

In the last step we have assumed that the line profile of the transitions is very narrow, $g(\omega_k) = \delta(\omega_k - \omega_{ba})$, compared to the spectral bandwidth of the radiation which induces the transition. We shall present in Chap. 10 a simple recipe to modify the result for narrow band radiation.

We see now, that in the final step the normalization volume L^3 has happily dropped out, since normalization of the field operator cancels versus mode density. We have written (2.149) in a manner to show the essential ingredients: apart from the numerical prefactor we recognize the *mode density per angle and volume* (2.75), the *dipole transition moment projected on the polarization* (2.134), \widehat{D}_{ba} , and the *total photon energy* $\mathcal{N}_{ke} \hbar \omega_{ba}$, with \mathcal{N}_{ke} being the number of photons in the mode \mathbf{k}, \mathbf{e} prior to absorption or emission with an angular frequency corresponding to the transition frequency ω_{ba} .

For emission we obtain correspondingly

$$dR_{ab} = d\Omega \frac{\pi e^2}{\varepsilon_0 \hbar^2} \frac{\omega_{ba}^2}{(2\pi c)^3} |\widehat{D}_{ab}|^2 (\mathcal{N}_{ke} + 1) \hbar \omega_{ba}. \quad (2.150)$$

We point out that this differs from (2.149), valid for absorption, by the *replacement* $\mathcal{N}_{ke} \rightarrow (\mathcal{N}_{ke} + 1)$. As we shall see in a moment, *this is crucial for spontaneous emission*.

According to (2.149) it is evident that the atom can only be excited from the lower state $|a\rangle$ into the upper state $|b\rangle$ if $\mathcal{N}_{ke} > 0$ – that is, if at least one photon of the frequency ω_{ba} is present in the field mode \mathbf{k}, \mathbf{e} . The absorption process reduces this number of photons by exactly one. Let us assume now that the number of photons \mathcal{N}_{ke} in the mode \mathbf{k}, \mathbf{e} is very high – so high that the relative uncertainty $1/\sqrt{\mathcal{N}_{ke}}$ about that number is negligible. Then \mathcal{N}_{ke} may be set equal to its average value according to (2.84) for all relevant modes. We insert this value – as indicated by [] – into (2.149):

$$\begin{aligned} R_{ba} &= \int_{\text{beam}} d\Omega \frac{\pi e^2}{\varepsilon_0 \hbar^2} \frac{\omega_{ba}^2}{(2\pi c)^3} |\widehat{D}_{ba}|^2 \left[\frac{\tilde{I}(\omega_{ba})}{\hbar \omega_{ba} c \delta\Omega} \frac{(2\pi c)^3}{\omega_{ba}^2} \right] \hbar \omega_{ba} \\ &= \frac{\pi e^2}{\varepsilon_0 c \hbar^2} \int_{\text{beam}} d\Omega |\widehat{D}_{ba}|^2 \frac{\tilde{I}(\omega_{ba})}{\delta\Omega}. \end{aligned}$$

We point out that the mode density and the single photon energy cancel out. The spectral intensity $\tilde{I}(\omega_{ba})$ is a measurable source parameter. E.g., its value is given by (2.21) for a laser tuned into resonance ω_{ba} – if its overall bandwidth is much larger than the linewidth of the transition.

We now recall that $|\widehat{D}_{ba}|^2 = |\mathbf{r}_{ba} \cdot \mathbf{e}|^2$ depends on the propagation direction of the light. For any reasonable laser beam, well collimated to $\delta\Omega \ll 1$, we may consider $|\mathbf{r}_{ba} \cdot \mathbf{e}|^2$ to be constant for all populated wave vectors \mathbf{k} in the beam. Under such conditions the angular dependence of $\tilde{I}(\omega_{ba})/\delta\Omega$ may be considered a delta function (beam) and the integration of (2.149) over all solid angles yields the *total absorption probability*

$$R_{ba} = \frac{\pi e^2}{\varepsilon_0 \hbar^2} |\widehat{D}_{ba}|^2 \frac{\tilde{I}(\omega_{ba})}{c} = \frac{4\pi^2 \alpha}{\hbar} |\widehat{D}_{ba}|^2 \tilde{I}(\omega_{ba}) = B_{ba} \frac{\tilde{I}(\omega_{ba})}{c} \quad (2.151)$$

with the *fine structure constant* $\alpha = e^2/4\pi\varepsilon_0 c \hbar$ and $B_{ba} = 4\pi^2 \alpha c |\widehat{D}_{ba}|^2/\hbar$, the EINSTEIN coefficient for the specific sub-transition $b \leftarrow a$ induced with polarization \mathbf{e} . We note that this expression is completely identical to (4.63), Vol. 1, derived in our previous semiclassical treatment. The rate R_{ba} (dimension T^{-1}) is – as already mentioned earlier – by a *factor of 3 larger than usually given in textbooks*, since we have derived the expression for a laser beam, rather than for isotropic radiation.

Of particular interest is now the *emission of a photon* in the transition $|b\rangle \rightarrow |a\rangle$. The factor $(\mathcal{N}_{ke} + 1)$ in (2.150) suggests to distinguish between induced and spontaneous emission: the *induced emission probability* is taken proportional to \mathcal{N}_{ke} ,

that is to the number of photons in the relevant modes prior to the emission process. A comparison of (2.149) and (2.150) shows, that this probability is identical to the absorption probability. Thus, for *one* well defined upper and *one* well defined lower state $|b\rangle$ and $|a\rangle$

$$R_{ab} = R_{ba}. \quad (2.152)$$

We note in passing, that the photons generated by induced emission appear by definition exactly in the mode by which they are created – as we have partitioned the whole radiation field (in \mathbf{k} space) into well defined, discrete modes and treated them independently prior to integration. This confirms what in the semiclassical treatment has simply be assumed: *radiation due to induced emission agrees in frequency and direction exactly with the inducing field.*

The factor $(\mathcal{N}_{ke} + 1)$ in (2.150) implies that emission may occur even if there is initially no field present, or more precisely, if initially the field is describe by the vacuum state with $\mathcal{N}_{ke} = 0$ (the initial state being $|b0\rangle$). There is an additional finite, albeit small probability for the de-excitation process $|b\rangle \rightarrow |a\rangle$, involving the emission of a photon. This transition may be seen as *induced by the vacuum field*. This notion may appear somewhat difficult to accept and we shall come back to it in the next subsection.

In any case, according to (2.150) the resulting *spontaneous transition probability* for emission of a photon into a mode \mathbf{k} with a frequency ω_{ba} and polarization \mathbf{e} into a solid angle $d\Omega$ is:

$$dR_{ab}^{(\text{spont})} = \frac{\pi e^2}{\varepsilon_0 \hbar^2} \frac{\omega_{ba}^2}{(2\pi c)^3} |\widehat{D}_{ab}|^2 \hbar \omega_{ba} d\Omega = \frac{\alpha \omega_{ba}^3}{2\pi c^2} |\widehat{D}_{ab}|^2 d\Omega. \quad (2.153)$$

We recall that we had “gleaned” this expression as (4.67), Vol. 1 for spontaneous emission earlier on. Above derivation supplements the proof.

However, we cannot confine the derivation to just one mode: all empty modes of frequency ω_{ba} do indeed contribute to the process. The angular distribution of this radiation and its polarization is described by $|\widehat{D}_{ba}|^2 = |\mathbf{r}_{ba} \cdot \mathbf{e}|^2$ (for details we refer to Sect. 4.5 in Vol. 1). While our earlier treatment of spontaneous emission was essentially guesswork, it is now firmly based on the quantized radiation field. The integration over all solid angles gives again the characteristic factor $8\pi/3|\mathbf{r}_{ba}|^2$, so that the total spontaneous emission rate becomes

$$R_{ab}^{(\text{spont})} = \sum_e \int_{4\pi} dR_{ab}^{(\text{spont})} = \frac{4\alpha}{3c^2} |\mathbf{r}_{ba}|^2 \omega_{ba}^3 = A_{ab} = \frac{1}{\tau_{ab}}. \quad (2.154)$$

A_{ab} refers here to spontaneous decay of a specific excited sub-state $|b\rangle$ into the specific lower sub-state $|a\rangle$ and fully confirms (4.109), Vol. 1, onto which we have based up to now all discussions and applications of the A coefficients. To obtain the overall natural lifetime τ_{nat} of a level, one has to sum this expression also over all final states. Detailed evaluation of the A and B coefficients for specific transitions

and the generalization to degenerate levels has already been presented in Sect. 4.4, Vol. 1.

We thus have achieved not less than an *ab initio* derivation of spontaneous emission and of the relation between the EINSTEIN *coefficients*. We can now trace the origin of the *well known* ω^3 *dependence of spontaneous emission*: It arises from the mode density (2.75), which is $\omega^2/(2\pi c^3)$ per unit volume and per angular frequency – and from the photon energy $\hbar\omega$. In the treatment of induced probabilities both terms cancel against the number of photons *per mode* and the spectral intensity per frequency interval. *Thus, the induced rate (2.151) does not depend directly on ω – except through the resonance condition $g(\omega_k) = \delta(\omega_k - \omega_{ba})$ in (2.149).*

Finally, we also have to realize the limitations of the present treatment for emission and absorption of electromagnetic radiation: we only have used 1st order perturbation theory. For induced processes we shall correct this to some extent in Chap. 10. We shall show there that the set of coupled equations (2.142) and (2.143) may be solved exactly, as long as the RWA holds, and spontaneous emission can be neglected. For intense (but not too intense) laser fields and times short compared to the natural lifetime this is indeed an excellent approximation. For very high intensities – as available today with state-of-the-art ultra fast, high power laser systems, the rotating wave approximation breaks down, and similarly perturbative approaches are of limited value only. Hence, special strong field approximations or brute force numerical methods must be applied.

As for spontaneous emission, it is of fundamental importance for any more rigorous treatment of radiative problems, and warrants further efforts beyond 1st order perturbation theory. The problem is, that the *initial conditions* (2.147) are, at a closer look, not strictly valid if spontaneous emission is to be included: *All empty modes are present at time zero*. It is important to realize that these empty modes are not nothing, but represent the vacuum field which is (almost) always present. Indeed, the vacuum field associated with these many unoccupied modes close to resonance leads to a broadening of the excited states which we know as *natural linewidth*. A quantitative treatment can be achieved in 2nd order perturbation theory – but is somewhat involved, and we refrain from presenting it here.

The result is, as already assumed in Chap. 5, Vol. 1, that $g(\omega)$ in (2.146) and (2.148) can no longer be treated as a δ -function. Rather, it has to be described by a LORENTZ profile with a linewidth (FWHM) $\Delta\omega_{\text{nat}} = A_{ab} = 1/\tau_{\text{nat}}$. With today's techniques the bandwidth of lasers used in spectroscopy may easily be kept much below that value. This implies that also our assumptions for deriving the relevant expression (2.151) for induced processes do no longer hold. However, as we shall show in Chap. 10 this particular problem may be cured by a small modification.

2.3.7 Spontaneous Emission in a Cavity

In order to obtain a quantized form of the radiation field we have introduced a very large but finite normalization volume. This has led us to discrete radiation modes – still infinitely many, but countable. And all these modes ‘own’ a characteristic vac-

uum field. It is this very vacuum field that we hold responsible for spontaneous emission.

Many other physical phenomena are also caused or influenced by the vacuum field (one speaks of *radiative corrections*). We recall the LAMB shift or the $g - 2$ anomaly of the electron magnetic moment treated in Chap. 6, Vol. 1, for which radiative corrections are held responsible. Nevertheless, the vacuum state is not a really trivial concept. It is by no means empty space, its eigenenergy being $\hbar\omega_k/2$ according to (2.114) – for each mode \mathbf{k} . Quantum electrodynamics deals with the problem of this infinite energy by its specific recipe for “re-normalization”. But of course, one might pose the question: *How real is this vacuum field?* Is it perhaps just a mathematical construct made to give the right answers for spontaneous emission?

What may happen, if one forcefully chooses experimental conditions so that the normalization volume cannot be made infinitively large? What if we confine any potential radiation to a small volume and let it interact there with an excited atom? What does “vacuum state” mean in such a case? The idea of such an experiment has been around for some time (see e.g. PURCELL 1946; KLEPPNER 1981). However, it became feasible only by modern lasers and sophisticated experimental techniques.

The first experiment of this type was performed by GOY et al. (1983) – and finally led, loosely speaking, to the NOBEL prize for HAROCHE and WINELAND (2012). They studied Na RYDBERG atoms, prepared by two photon resonant excitation in the $23s$ state, and investigated its spontaneous decay to the $22p$ state in a microwave cavity. The dipole transition moment between such high n levels is very high, while at the same time the spontaneous transition probability in free space is very small, being proportional to $\propto \nu^3$. In the case discussed here the transition frequency is $\nu = 341$ GHz (as one easily verifies with the quantum defects of Na given in Table 3.4, Vol. 1). The spontaneous decay rate between the $23s$ and $22p$ levels is only $\tau_{22p23s} = 150\text{s}^{-1}$. At this transition wavelengths ($\lambda = 0.88$ mm) super-conducting microwave resonators with extremely high finesse can be built, through which an atomic beam can pass without problems.

Figure 2.20(a) shows a very schematic summary of the experimental setup. A low density sodium beam passes through the microwave cavity where the atoms are excited in a two photon process by 2 collinear, pulsed (5 ns) dye laser beams, entering the resonator perpendicular to the Na-beam and to the resonator mode. The RYDBERG atoms are detected by field ionization in a parallel plate capacitor to which (after the laser pulse) a ramp voltage is applied as indicated in Fig. 2.20(b). The ionization process is monitored very efficiently by detecting the ejected electrons with an electron multiplier. Atoms with the lower ionization potential $W_I(23s)$ are ionized at a lower field strength (i.e. earlier) than those with higher ionization potential $W_I(22p)$. In the detected ionization signal, Fig. 2.20(c), atoms in the $23s$ state are recorded first, $22p$ atoms appear later. The black signal trace is taken with the cavity out of resonance for the $22p \leftarrow 23s$ transition. The cavity may be tuned into resonance mechanically, but fine adjustment is done by a small electric field in the cavity which can STARK shift the $22p$ levels slightly. The actual experiment is carried out with only a few (1–3) excited atoms in the cavity, so that they do not influence each other. The red line shows the signal with the cavity tuned into reso-

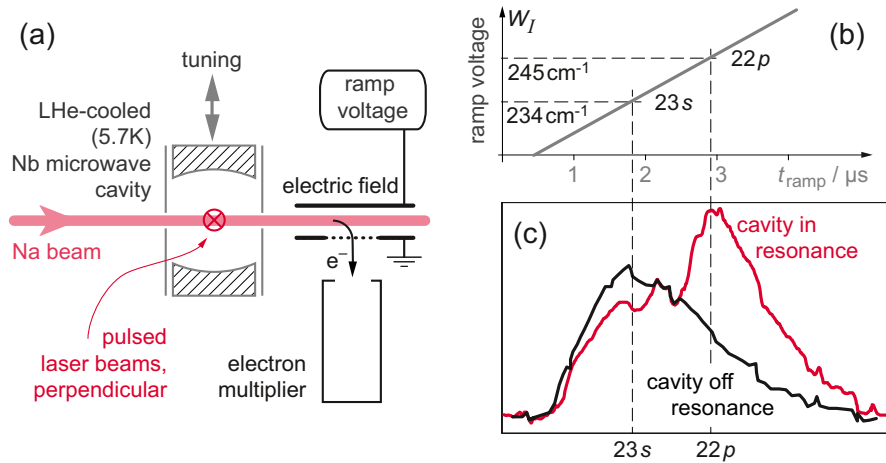


Fig. 2.20 Experiment of GOY et al. (1983) documenting spontaneous transitions between Na $23s \rightarrow 22p$ levels in a microwave cavity. (a) Setup very schematically, (b) ramp voltage tuning to detect $23s$ or $22p$ levels, (c) experimental signal taken from Fig. 3a in GOY et al. (1983), showing the signal measured when the cavity is off resonance (black line) and on resonance (red line)

nance: a surprisingly intense signal originates from atoms in the $22p$ state – which is attributed to spontaneous emission in the cavity.

This is fascinating result! To fully understand it we first have a closer look at the cavity. It is made of very precisely machined and highly polished, niobium spheres with 20 mm diameter and 26 mm radius of curvature, arranged in nearly confocal configuration at $L = 25 \text{ mm}$ distance. The Gaussian mode sustained by the cavity at $\lambda = 0.88 \text{ mm}$ has a waist $w = 1.9 \text{ mm}$ and a total volume of $V_{\text{cav}} = L\pi w^2/4 = 70 \text{ mm}^3$. Nb becomes super-conducting at 9.2 K and the cavity is liquid He cooled to ca. 5.7 K. This ensures that the surface of the cavity is highly conducting and together with very good polishing this leads to a very high quality factor Q of the cavity (see Eq. (1.11)) on the order of 10^6 . In addition, the cooling ensures that black body background radiation cannot lead to induced transitions: according to (1.63), Vol. 1, BOSE-EINSTEIN statistics gives a population of the $\mathcal{N} = 1$ mode of $[\exp(\hbar\omega/k_B T) - 1]^{-1} \simeq 0.06$ relative to the vacuum state $\mathcal{N} = 0$ so that radiation induced processes can be neglected compared to spontaneous transitions which are caused by the vacuum field. We emphasize the fact that no external or background microwave field is involved in this experiment.

The atoms spent only about $2 \mu\text{s}$ in the resonant cavity mode. In the free field case this would lead to a maximum of $150 \text{ s}^{-1} \times 2 \mu\text{s} \simeq 3 \times 10^{-4}$ transitions. How then can we understand the observed enhancement of spontaneous emission by about at least 5 orders of magnitude?

From our derivation of spontaneous emission in the free field case we recall now, that one crucial parameter was the *mode density per unit volume*, according to (2.75) $\rho_{\text{free}}(\omega) = \omega_{ba}^2 / (2\pi c)^3$. This has entered directly into the spontaneous emission rate (2.153). In the final step, integration over all angles leads to multiplication by a

factor of $8\pi/3$, and another factor of 2 for the two possible polarization modes. We now compare this to the situation in the cavity. The mode density per angular frequency, polarization and volume is $\rho_{\text{cav}}(\omega) = 1 \text{ mode}/(V_{\text{cav}} \Delta\omega_r)$, where V_{cav} is the cavity volume and $\Delta\omega_r = \omega_r/Q$ with the Q factor of the cavity according to (1.11). Integration over solid angles is obsolete in this case, since the cavity sustains only two modes (of different polarization) which are resonant with the transition. In summary, one has to replace $2 \times (8\pi/3) \rho_{\text{free}}(\omega)$ in free space by $2 \times \rho_{\text{cav}}(\omega)$ in the resonant cavity case. Thus, an enhancement of the spontaneous radiation probability

$$\frac{\rho_{\text{cav}}(\omega)}{(8\pi/3) \rho_{\text{free}}(\omega)} = \frac{Q}{V_{\text{cav}} \omega_{ba}} \frac{(2\pi c)^3}{(8\pi/3) \omega_{ba}^2} = \frac{1}{V_{\text{cav}}} \frac{3Q}{4\pi} \lambda^3$$

is expected. In the present case this enhancement factor is on the order of 10^3 , so that the transition probability is changed from 150 s^{-1} to $\simeq 3 \times 10^5 \text{ s}^{-1}$ so that during the passage time of $2 \mu\text{s}$ a substantial fraction of the Na atoms in the initial 23s state decays by spontaneous transitions into any of the $22p$ substates – as shown by the experimental result Fig. 2.20(c).

In conclusion, this experiment documents that the vacuum field is not just a theoretical construct, it is real and can be manipulated in a finite cavity – leading to an observable modification of the spontaneous transition probability – also reflected in the respective “natural” lifetime.

A number of additional questions arise from these findings: e.g. what happens to the emitted photon? Can spontaneous emission also be suppressed? What about other effects caused by the vacuum field in a cavity? As it turns out, in the experiment described here the Q factor of the cavity is not high enough to store the emitted photon long enough for subsequent reabsorption.

In the mean time, experiments have been reported in which oscillatory energy between the cavity and a single atom in it has been observed. And, yes, spontaneous emission can also be quenched in a cavity of the right dimensions if the vacuum field is not in resonance. Also changes of atomic energy levels and modifications of the LAMB shift have been observed. *Cavity quantum electrodynamics* has become a very active and productive topic of modern research as e.g. summarized in a nice review by WALTHER et al. (2006). We also mention that such effects play an important role in *nano-optics*, another area of cutting edge research.

Section summary

- We have quantized the electromagnetic field, based on the preceding introduction of discrete, countable modes of the electromagnetic radiation field in a large, but finite normalization volume L^3 .
- To this end we have introduced in (2.92) new variables P and Q as linear combinations of the components E^- and E^+ of the electric field. The mode energy was then recognized as formally equivalent to the harmonic oscillator, with P and Q being canonic conjugate coordinates.

- We have applied the standard quantization scheme, replacing these variables by operators with the commutation rule $[\hat{Q}, \hat{P}] = i\hbar$. Back transformation led us to operators \hat{a}^+ and \hat{a} , the so called *creation and annihilation operators*, for which the commutation rule $[\hat{a}, \hat{a}^+] = 1$ holds.
- The Hamiltonian for a single mode of the free electromagnetic field is

$$\hat{H}_F = \hbar\omega_k(\hat{a}^+\hat{a} + 1/2).$$

It has eigenstates $|\mathcal{N}\rangle$, with \mathcal{N} representing the number of photons in that particular mode of energy $\hbar\omega_k$. The mode energies correspond to those of the harmonic oscillator $W_{\mathcal{N}} = (\mathcal{N} + \frac{1}{2})\hbar\omega_k$.

- The operator $\hat{N} = \hat{a}^+\hat{a}$ counts the number \mathcal{N} of photons in a mode and the creation and annihilation operators \hat{a}^+ and \hat{a} , respectively, were found to raise or decrease \mathcal{N} by one.
- The total Hamiltonian of the free field is the sum of the Hamiltonians for all modes. This scheme of writing the Hamiltonian is called *second quantization*.
- The components \hat{E}^+ and \hat{E}^- of the electric field operator (2.112) are proportional to \hat{a}^+ and \hat{a} , respectively. In the SCHRÖDINGER picture all operators are independent of time. All time dependence of the problem, being $\propto \exp[-iW_{\mathcal{N}}t/\hbar]$, has been cast onto the states.
- We have briefly introduced GLAUBER states (2.115), representing a coherent electromagnetic field. They are eigenstates of the negative component of the electric field operator \hat{E}^- . Some of their properties have been described in Sect. 2.3.3.
- The interaction between the atom and field has been written in full analogy to the semiclassical treatment as $\hat{U}(\mathbf{r}) = e\mathbf{r} \cdot \hat{\mathbf{E}}$, independent of time. Thus, the problem is now formulated energy conserving: energy is just exchanged between the atom and the electromagnetic field.
- Transition probabilities were treated again in 1st order perturbation theory. The number of photons per mode, \mathcal{N}_{ke} , appears in the transition rates. We have identified it with the mean number of photons per mode as derived in the previous section.
- Specifically, for de-excitation processes the rate was found to be proportional to $\mathcal{N}_{ke} + 1$. This implies that de-excitation is possible even if there is no external field. This has allowed us to derive a quantitative expression (2.154) for spontaneous emission.
- We thus have concluded that spontaneous transitions are induced by the vacuum field. *The vacuum state is not simply nothing!* Its energy is $\hbar\omega_k/2$ in each mode, and the vacuum field is a physically present field.
- Experimentally this may be verified in a high Q cavity, where the vacuum field can be manipulated. Spontaneous emission is found to be enhanced or suppressed in such a cavity, depending on whether the mode is on or off resonance with the transition.

Acronyms and Terminology

chemical-potential: ‘In statistical thermodynamics defined as the amount of energy or work that is necessary to change the number of particles of a system (by 1) without disturbing the equilibrium of the system’, see μ in Sect. 1.3.4, Vol. 1.

CW: ‘Continuous wave’, (as opposed to pulsed) light beam, laser radiation etc.

E1: ‘Electric dipole’, transitions induced by the interaction of an electric dipole with the electric field component of electromagnetic radiation.

E2: ‘Electric quadrupole’, transitions induced by the interaction of a quadrupolar charge distribution with the electromagnetic radiation field.

EPR: ‘Electron paramagnetic resonance’, spectroscopy, also called *electron spin resonance* ESR (see Sect. 9.5.2 in Vol. 1).

ESO: ‘European southern observatory’, in Chile, hosting four of today’s largest telescopes of the world, with 8.5 m diameter each.

esu: ‘electrostatic units’, old system of unities, equivalent to the GAUSS system for electric quantities (see Appendix A.3 in Vol. 1).

FPI: ‘FABRY-PÉROT interferometer’, for high precision spectroscopy and laser resonators (see Sect. 6.1.2 in Vol. 1).

FWHM: ‘Full width at half maximum’.

HBT: ‘Hanbury BROWN and TWISS’, experiment, to determine the lateral correlation of light by a second-order interferometric measurement (see Sect. 2.1.6).

IR: ‘Infrared’, spectral range of electromagnetic radiation. Wavelengths between 760 nm and 1 mm according to ISO 21348 (2007).

M1: ‘Magnetic dipole’, transitions induced by the interaction of a magnetic dipole with the magnetic field component of electromagnetic radiation.

NIR: ‘Near infrared’, spectral range of electromagnetic radiation. Wavelengths between 760 nm and 1.4 μm according to ISO 21348 (2007).

NMR: ‘Nuclear magnetic resonance’, spectroscopy, a rather universal spectroscopic method for identifying molecules (see Sect. 9.5.3 in Vol. 1).

QED: ‘Quantum electrodynamics’, combines quantum theory with classical electrodynamics and special relativity. It gives a complete description of light-matter interaction.

RF: ‘Radio frequency’, range of the electromagnetic spectrum. Technically, one includes frequencies from 3 kHz up to 300 GHz or wavelengths from 100 km to 1 mm; ISO 21348 (2007) defines the RF wavelengths from 100 m to 0.1 mm; in spectroscopy RF usually refers to 100 kHz up to some GHz.

RWA: ‘Rotating wave approximation’, allows to solve the coupled equations for a two level system in a strong electromagnetic field in closed analytical form (see Sect. 10.2.3).

SHG: ‘Second harmonic generation’, doubling of a fundamental frequency, for infrared or visible light typically by methods of nonlinear optics.

UV: ‘Ultraviolet’, spectral range of electromagnetic radiation. Wavelengths between 100 nm and 400 nm according to ISO 21348 (2007).

VIS: ‘Visible’, spectral range of electromagnetic radiation. Wavelengths between 380 nm and 760 nm according to ISO 21348 (2007).

VLBI: ‘Very long baseline interferometry’, worldwide network of radio telescopes for interferometry.

References

- BAYM, G.: 1998. ‘The physics of Hanbury Brown-Twiss intensity interferometry: From stars to nuclear collisions’. *Acta Phys. Pol. B*, **29**, 1839–1884.
- BETH, R. A.: 1936. ‘Mechanical detection and measurement of the angular momentum of light’. *Phys. Rev.*, **50**, 115–125.
- BORN, M. and E. WOLF: 2006. *Principles of Optics*. Cambridge: Cambridge University Press, 7th (expanded) edn.
- BOYAJIAN, T. S. et al.: 2012. ‘Stellar diameters and temperatures. I. Main-sequence A, F, and G stars’. *Astrophys. J.*, **746**, 101 (26 pages).
- BROWN, R. H. and R. Q. TWISS: 1954. ‘A new type of interferometer for use in radio astronomy’. *Philos. Mag.*, **45**, 663–682.
- BROWN, R. H. and R. Q. TWISS: 1956a. ‘Correlation between photons in 2 coherent beams of light’. *Nature*, **177**, 27–29.
- BROWN, R. H. and R. Q. TWISS: 1956b. ‘A test of a new type of stellar interferometer on Sirius’. *Nature*, **178**, 1046–1048.
- BROWN, R. H. and R. Q. TWISS: 1958. ‘Interferometry of the intensity fluctuations in light II. An experimental test of the theory for partially coherent light’. *Proc. R. Soc. A* **243**, 291–319.
- TEN BRUMMELAAR, T. A. et al.: 2005. ‘First results from the Chara array. II. A description of the instrument’. *Astrophys. J.*, **628**, 453–465.
- DAVIS, J. and B. LOVELL: 2003. ‘Robert Hanbury Brown, 1916–2002’, Australian Academy of Science. <http://www.science.org.au/fellows/memoirs/brown.html>, accessed: 9 Jan 2014.
- GLAUBER, R. J.: 1963. ‘Coherent and incoherent states of radiation field’. *Phys. Rev.*, **131**, 2766–2788.
- GLAUBER, R. J.: 2005. ‘The NOBEL prize in physics: for his contribution to the quantum theory of optical coherence’, Stockholm. http://nobelprize.org/nobel_prizes/physics/laureates/2005/.
- GLAUBER, R. J.: 2006. ‘NOBEL lecture: 100 years of light quanta’. *Rev. Mod. Phys.*, **78**, 1267–1278.
- GLAUBER, R. J.: 2007. *Quantum Theory of Optical Coherence, Selected Papers and Lectures*. New York: Wiley-VCH Verlag, 643 pages.
- GOY, P., J. M. RAIMOND, M. GROSS and S. HAROCHE: 1983. ‘Observation of cavity-enhanced single-atom spontaneous emission’. *Phys. Rev. Lett.*, **50**, 1903–1906.
- GRANGIER, P., G. ROGER and A. ASPECT: 1986. ‘Experimental-evidence for a photon anticorrelation effect on a beam splitter – a new light on single-photon interferences’. *Europhys. Lett.*, **1**, 173–179.
- GRYNBERG, G., A. ASPECT and C. FABRE: 2010. *Introduction to Quantum Optics: From the Semi-classical Approach to Quantized Light*. Cambridge: Cambridge University Press, 665 pages.
- HAROCHE, S. and D. J. WINELAND: 2012. ‘The NOBEL prize in physics: for ground-breaking experimental methods that enable measuring and manipulation of individual quantum systems’, Stockholm. http://www.nobelprize.org/nobel_prizes/physics/laureates/2012/.
- HASSELBACH, F.: 2010. ‘Progress in electron- and ion-interferometry’. *Rep. Prog. Phys.*, **73**.
- HENNY, M., S. OBERHOLZER, C. STRUNK, T. HEINZEL, K. ENSSLIN, M. HOLLAND and C. SCHONENBERGER: 1999. ‘The fermionic Hanbury Brown and Twiss experiment’. *Science*, **284**, 296–298.
- ISO 21348: 2007. ‘Space environment (natural and artificial) – Process for determining solar irradiances’. *International Organization for Standardization*, Geneva, Switzerland.
- JELTES, T. et al.: 2007. ‘Comparison of the Hanbury Brown-Twiss effect for bosons and fermions’. *Nature*, **445**, 402–405.

- KIMBLE, H. J., M. DAGENAIS and L. MANDEL: 1977. 'Photon anti-bunching in resonance fluorescence'. *Phys. Rev. Lett.*, **39**, 691–695.
- KLEPPNER, D.: 1981. 'Inhibited spontaneous emission'. *Phys. Rev. Lett.*, **47**, 233–236.
- KLEPPNER, D.: 2008. 'Hanbury Brown's steamroller'. *Phys. Today*, **61**, 8–9.
- LAMBROPOULOS, P. and D. PETROSYAN: 2007. *Fundamentals of Quantum Optics and Quantum Information*. Berlin, Heidelberg, New York: Springer Verlag, 325 pages.
- LOUDON, R.: 2000. *Quantum Theory of Light*. Oxford, New York: Oxford University Press, 3rd edn.
- MANDEL, L. and E. WOLF: 1995. *Optical Coherence and Quantum Optics*. Cambridge: Cambridge University Press.
- MICHELSON, A. A. and F. G. PEASE: 1921. 'Measurement of the diameter of a orionis with the interferometer'. *Astrophys. J.*, **53**, 249–259.
- MILLONI, P. W. and J. H. ÉBERLY: 2010. *Laser Physics*. Hoboken: Wiley, 832 pages.
- MONNIER, J. D.: 2003. 'Optical interferometry in astronomy'. *Rep. Prog. Phys.*, **66**, 789–857.
- MUKAMEL, S.: 1999. *Principles of Nonlinear Optical Spectroscopy*. Oxford: Oxford University Press, 576 pages.
- PHILLIPS, D. T., H. KLEIMAN and S. P. DAVIS: 1967. 'Intensity-correlation linewidth measurement'. *Phys. Rev.*, **153**, 113–115.
- PURCELL, E. M.: 1946. 'Spontaneous emission probabilities at radio frequencies'. *Phys. Rev.*, **69**, 681, Note B10.
- WALTHER, H., B. T. H. VARCOE, B. G. ENGLERT and T. BECKER: 2006. 'Cavity quantum electrodynamics'. *Rep. Prog. Phys.*, **69**, 1325–1382.
- WEISSBLUTH, M.: 1978. *Atoms and Molecules*. New York, London, Toronto, Sydney, San Francisco: Academic Press, Student Edition, 713 pages.
- WEISSBLUTH, M.: 1989. *Photon-Atom Interactions*. New York, London, Toronto, Sydney, San Francisco: Academic Press, 407 pages.

Atoms, Molecules and Optical Physics 2

Molecules and Photons - Spectroscopy and Collisions

Hertel, I.V.; Schulz, C.-P.

2015, XXXV, 728 p. 393 illus., 383 illus. in color.,

Hardcover

ISBN: 978-3-642-54312-8